Late Cenozoic Exhumation in a Transpressional Setting: Fairweather Range, Alaska

Ryan Joseph McAleer

Thesis submitted to the faculty of the
Virginia Polytechnic Institute and State University
in partial fulfillment of the requirements for the degree of

Master of Science
In
Geosciences

James A. Spotila, Chair
John A. Hole
Richard D. Law

June 28, 2006
Blacksburg, Virginia

Keywords: Alaska, AHe dating, transpression, exhumation, glacial erosion

Late Cenozoic Exhumation in a Transpressional Setting: Fairweather Range, Alaska

Ryan J. McAleer

ABSTRACT

Deformation in southern Alaska is controlled by the accretion and partial subduction of the Yakutat terrane as margin-parallel motion transitions to subduction. Recent studies have shown that deformation in the St. Elias orogen, at the northern end of the terrane, accommodates a large portion of convergence, but deformation at the eastern and southern margins remains more poorly constrained. Rapid recent sedimentation (> 1cm/yr) and glacio-isostatic uplift rates (> 3 cm/yr) in the Fairweather corridor highlight short-term vertical deformation at the eastern margin; however, the relationship between these rates and long-term deformation is less well known.

New low-temperature cooling ages are reported along the eastern flank of the St. Elias orogen, placing constraints on vertical deformation over the past few million years. Young cooling ages (< 3 Ma) occur in a broad zone, extending along the onshore length of the strike-slip Fairweather fault. These ages indicate that protracted convergence has been accommodated in the Fairweather corridor. Average (~1 mm/yr) and peak (~3 mm/yr) late Cenozoic exhumation rates are similar to rates to the north, and suggest that the orogen is actually boomerang-shaped in map view. If ~1 mm/yr exhumation has been steady, the onset of rapid exhumation is constrained to post-12 Ma, but likely occurred at 5 Ma with changes in climate and plate obliquity. Although cooling ages reveal no coherent regional pattern relative to known structures, they indicate the margin accommodates a significant component of pure shear and is slip-partitioned. The resolved magnitude of convergence in the Fairweather corridor also indicates that Yakutat terrane motion is rotated from Pacific plate motion, and likely requires significant slip on the Transition fault at the southern edge of the Yakutat terrane. Although million-year exhumation rates are rapid, they are slower than short-term rates related to deglaciation.

Acknowledgements

"Nine tenths of education is encouragement."
-Anatole France

Without the encouragement of my parents I wouldn't be here today. For as long as I can remember you guys have been there in my corner. Whether it was late-night baseball games, life's decisions, or lincoln log houses your support and belief in me was always clear. I hope you know just how much that has meant and how proud I feel to be your son. Beth, what can I say, you are everything to me. No one knows me better and no one has to put up with more. Thank you for listening to me talk about rocks, thanks for correcting my grammar, staying up late to talk to me, driving 7 hours on no sleep to see me, cutting my hair, getting me books, making me schedules, bringing me Smith's hot dogs, introducing me to whole wheat pasta, writing me letters, and the list goes on (is this a run-on?). Without your love and patience there's no way I'd be where I am. Smile Beth, our later is finally here.

I'd like to thank my adviser Dr. Spotila. You put up with all of my antics and on occasion even partook in them. You were the perfect combination of scary boss and helpful educator, and you forced me to think for myself. I won't soon forget the sea of red that is a "Jim revised" draft, nor how good it felt when I got a compliment because I knew I had earned it. Your science is pure. Is there any better compliment? I'd also like to thank John Hole and Rick Law for being on my committee, and Ken Eriksson and John for revising my thesis. Thanks to the faculty and staff for many things. Thanks to my officemates. You guys have been awesome. Aaron, bouncing Alaska ideas off you was so helpful, and you never cease to amaze me with your enthusiasm for science. Your constant good attitude made my office days more bearable. Jamie—bearded clown and late-night office companion—your unparalleled sarcasm is no less than breathtaking. When I think of Parsely Goodmood I will think of you. And lastly, to all of my friends here, you made it two pretty wonderful years. Thanks for keeping me sane and I wish all of you the best.

Table of Contents

List of Tables and Figures

1. Introduction

The modern day deformation of southern Alaska is controlled by the accretion and partial subduction of the Yakutat terrane, a composite continental-oceanic block (e.g. Plafker et al., 1994). The majority of the convergence between the Yakutat terrane (YT) and stable North America (NA) is accommodated in the core of the St. Elias orogen between Yakutat Bay and Kayak Island (Sauber, 1997), where YT motion is highly oblique to the NA margin (Figure 1). Modern deformation in the orogenic core is exhibited by active thrusting, abundant seismicity, and geodetically observed surface motion (Liskowski, 1987, Sauber, 1997). Protracted late Cenozoic deformation is evidenced by a broad fold and thrust belt, some of North America's highest peaks (e.g. Mt. Logan, 5959 m) (Figure 2), ~5 km thick Plio-Pleistocene sediments (Lagoe et al., 1994), and young (U-Th)/He and fission-track cooling ages (O'Sullivan and Currie, 1996; Spotila et al., 2004; Johnston, 2005). However, despite the abundant evidence for continued late Cenozoic deformation, constraints on the distribution of deformation through time are lacking, resulting in largely conjectural evolutionary models of orogenesis. Additionally, observations made at different time scales and from different sources often produce seemingly contradictory results. One area where the mismatch between numerical modeling and geologic and geodetic data is particularly acute is along the Fairweather fault at the poorly studied eastern margin of the St. Elias orogen.

GPS-derived, nearly margin parallel motion of the YT (Fletcher and Freymueller, 1999) in conjunction with dextral motion along the Fairweather fault during a major rupture in 1958 (Tocher and Miller, 1959) suggest little contraction is currently accommodated at this margin. However, Pacific plate (PA) motion ~20° oblique to the NA margin (DeMets and Dixon, 1999), and the unknown coupling of the YT and PA along the Transition fault indicate the margin may be transpressive. Furthermore, geologic observations, such as high topography (e.g. Mt. Fairweather, 4663 m) (Figure 2) and a topographic escarpment (Pavlis et al., 2004), and young reconnaissance thermochronology along the northern Fairweather fault (O'Sullivan et al., 1997), suggest the margin has been transpressive in recent geologic time. Scattered apatite fission-track ages are especially intriguing, as they resolve cooling rates comparable to those recorded

in the core of the St. Elias orogen (Spotila et al., 2004) where ~3 cm/yr of YT-NA convergence is accommodated (Sauber et al., 1997). Moreover, uplifted Holocene marine terraces (Hudson et al., 1976), recently developed offshore anticlines, coseismic uplift during the 1899 Yakutat Bay earthquake (Plafker et al., 1994), and the world's highest, primarily glacioisostatic, active uplift rates (> 3 cm/yr) (Larsen et al., 2004) highlight the ongoing vertical deformation at the margin.

If YT motion is oblique to the Fairweather corridor, the orogen is not limited to the zone between the Yakutat Bay and the Kayak Island Zone. Instead, convergent deformation likely extends from the St. Elias Mountains to the south along the Fairweather margin, resulting in a boomerang-shaped orogen in map view. As such, many of the motivations for studying the core of the orogen apply to the zone surrounding the Fairweather fault.

The roles of extrusion, subduction, and crustal thickening during terrane accretion are not well understood. Analyses of ancient orogens have been used to suggest lateral movement often plays an important role in accommodating convergence during accretion (Vauchez and Nicolas, 1991). However, ancient orogens represent an end product. Thus, they fail to capture the evolution of structures and to relate deformation rates and style to boundary conditions in the lithosphere. As such, the timing, geometry, and location of orogen-parallel motion relative to active accretion are not well understood (Vauchez and Nicolas, 1991). Active YT accretion provides a unique opportunity to study these processes where lithospheric conditions can be constrained. YT accretion also provides an opportunity to study transpressional tectonics. If YT-PA motion parallels PA-NA motion, the expected degree of obliquity in the Fairweather corridor is similar (~20°) to motion at the oft studied Alpine (New Zealand) and San Andreas(California) faults (Big Bend area) where pure shear dominated transpression results in very different deformation styles (e.g. Teyssier et al., 1995). The fundamental mechanisms controlling lithospheric behavior during transpression are not understood (e.g. Teyssier et al., 1995), and deformation along the Fairweather fault provides additional empirical evidence of transpressive accommodation along continental strike-slip faults. Southern Alaska is also an ideal place to examine the complex interplay between surface processes and tectonics. The power of surface processes in southern Alaska is evidenced by rapid recent glacial

erosion and glacio-isostatic uplift rates. Coupled erosion-deformation models (e.g. Beaumont et al., 1992; Willet et al., 1993) suggest that such mass redistribution by surface processes may strongly influence deformation patterns in the lithosphere over the long-term. However, this relationship is difficult to prove. The protracted glaciation (Lagoe et al., 1993) of the St. Elias orogen provides an efficient long-term mechanism of erosion, and the lithospheric response to this erosion will further resolve the relative contributions of erosion and tectonics in a coupled system.

Here we examine the Late Cenozoic vertical accommodation of plate motion in the Fairweather corridor using thermochronometry. The low temperature cooling history of bedrock samples from across the area constrains recent denudation patterns and rates. Young (U-Th)/He apatite ages are documented along the entire Fairweather corridor, from Yakutat Bay to Glacier Bay, but no coherent age pattern along or across strike of the Fairweather fault is resolved. Young ages imply the margin is transpressive and slip-partitioned, however, the pattern suggests a different mechanism of exhumation than in the Southern Alps of New Zealand, and slower exhumation rates despite similar climate. Sample ages also indicate that the YT does not move at the PA azimuth, suggesting rotation of the YT compatible with models for extrusion to the west.

Figure Caption

Figure 1: Relief map of northwestern North America. Note the location of the Yakutat terrane at the abrupt change ("cusp") in plate margin orientation. The Kayak Island Zone (KIZ) and Yakutat Bay (YB) bound the core of the St. Elias Orogen. If convergence extends into the Fairweather corridor south of Yakutat Bay the orogen has a "boomerang" shape. Scale bar is approximate, as scale varies across the map. Approximate PA-NA velocities are from (DeMets and Dixon, 1999). Box indicates location of Figure 2. Based on elevation data freely available at the United States Geological Survey (USGS).

Figure 2: *a)* Map of southern Alaska. Inset figure shows the Fairweather fault-normal and Fairweather fault-parallel components of PA-NA motion (DeMets and Dixon, 1999). The dashed line represents GPS derived motion in the town of Yakutat ~ 50km outboard of the Fairweather fault (Fletcher and Freymueller, 2003). Locations of faults are from Plafker et al. (1994); KIZ-Kayak Island Zone; CSEF-Chugach St. Elias fault; PZ-Pamplona Zone; DRZ; Dangerous River Zone. Focal mechanisms for recent earthquakes are from Lahr et al. (1988) and Doser and Lomas (2000). Bullseyes represent zones of maximum current uplift as measured by GPS (Larsen et al., 2005). *b)* Holocene uplift rates derived from raised terraces in Lituya Bay (data from Hudson et al., 1976). *c)* Cross section of July, 1973 earthquakes near Cross Sound (data from Doser and Lomas, 2000). The locations and senses of motion are compatible with underthrusting at the Transition fault zone (TFZ).

Figure 1

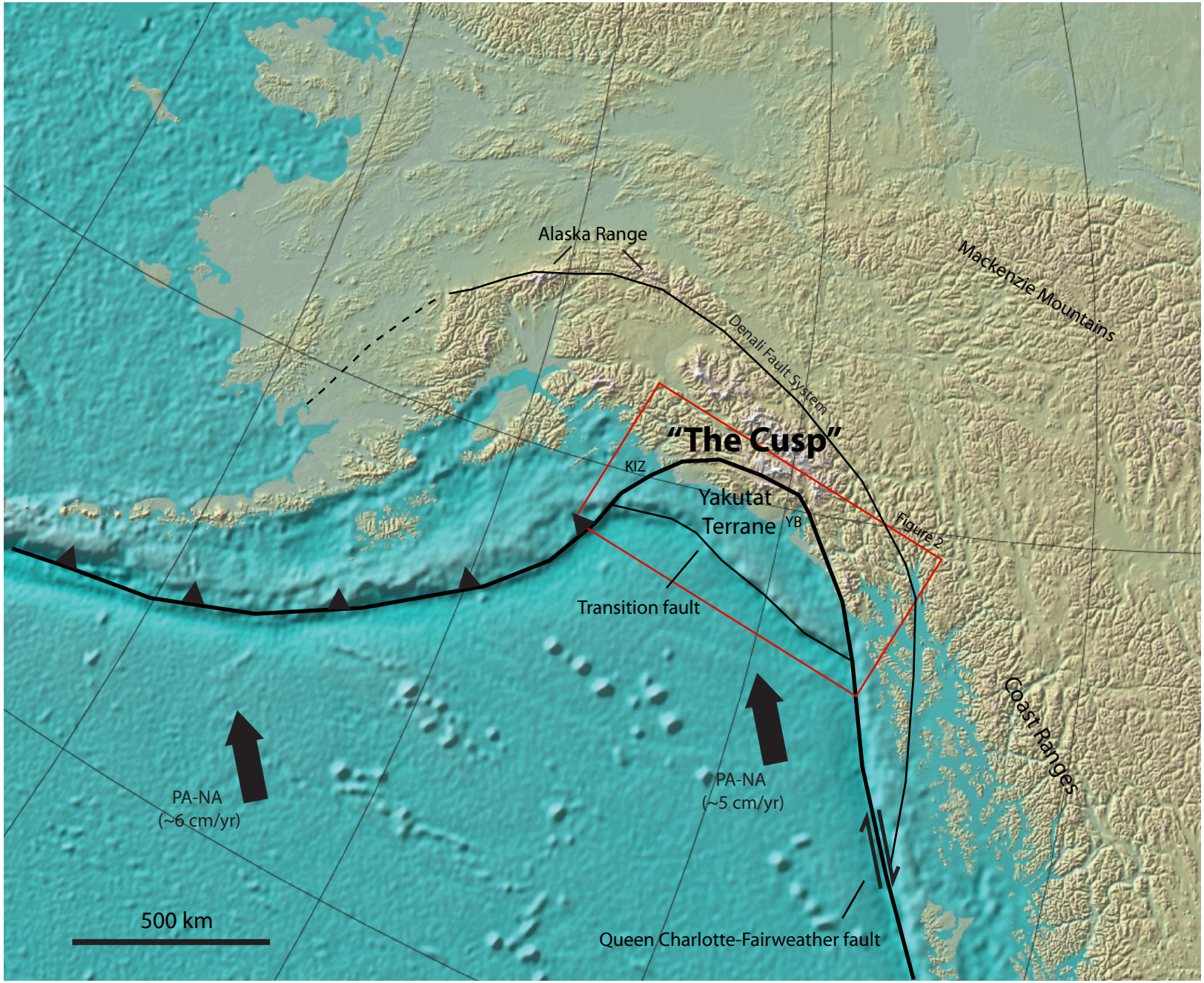
Alaska Range
Mackenzie Mountains
Denali Fault System
"The Cusp"
KIZ
Yakutat
Terrane
YB
Figure 2
Transition fault
Coast Ranges
PA-NA
(~6 cm/yr)
PA-NA
(~5 cm/yr)
500 km
Queen Charlotte-Fairweather fault

Figure 2

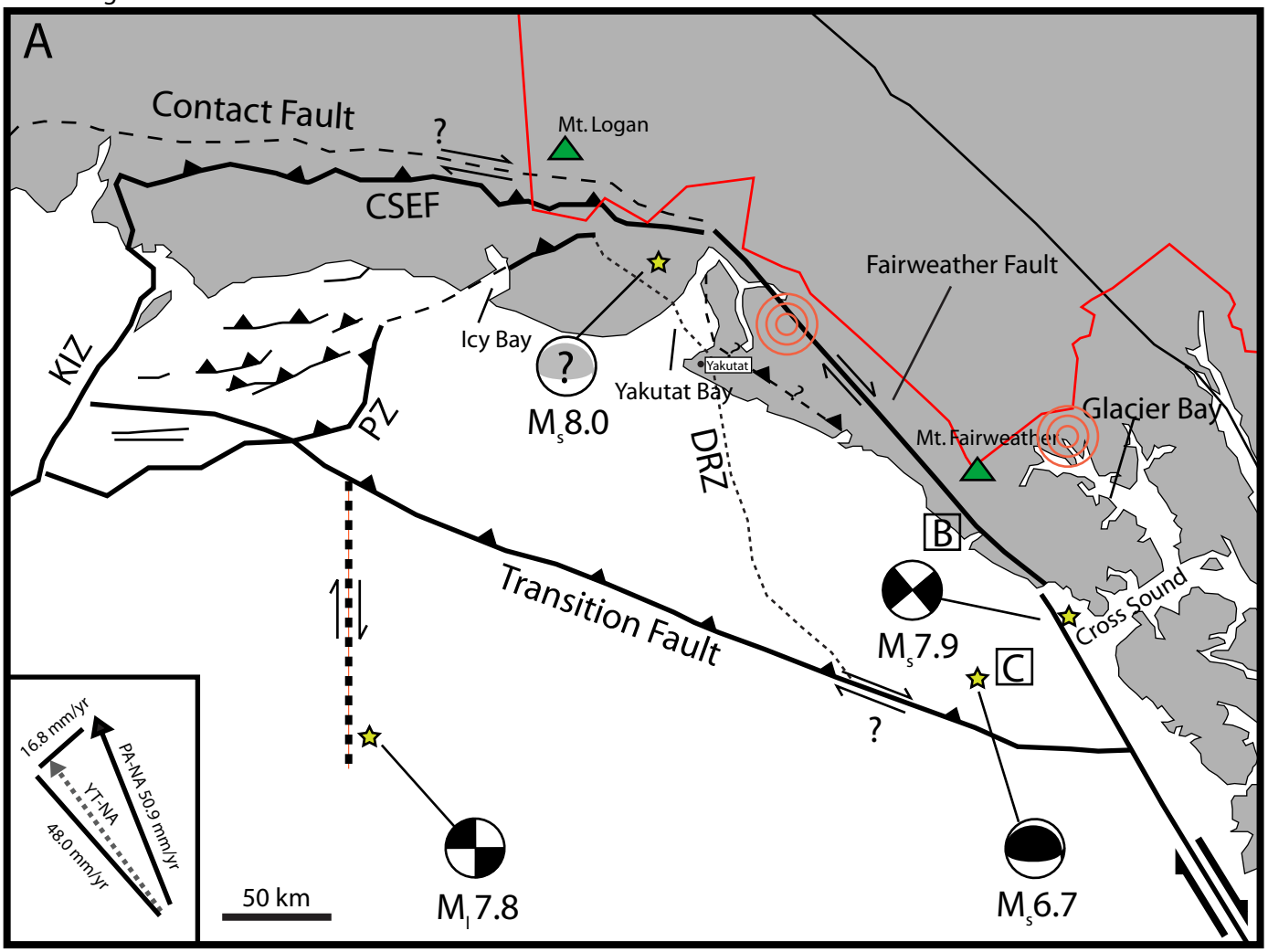
A
Contact Fault
?
Mt. Logan
CSEF
Fairweather Fault
Icy Bay
?
Yakutat
Yakutat Bay
Glacier Bay
KIZ
PZ
DRZ
M$_s$8.0
Mt. Fairweather
B
Transition Fault
M$_s$7.9
Cross Sound
C
?
16.8 mm/yr
PA-NA 50.9 mm/yr
YT-NA
48.0 mm/yr
50 km
M$_l$7.8
M$_s$6.7

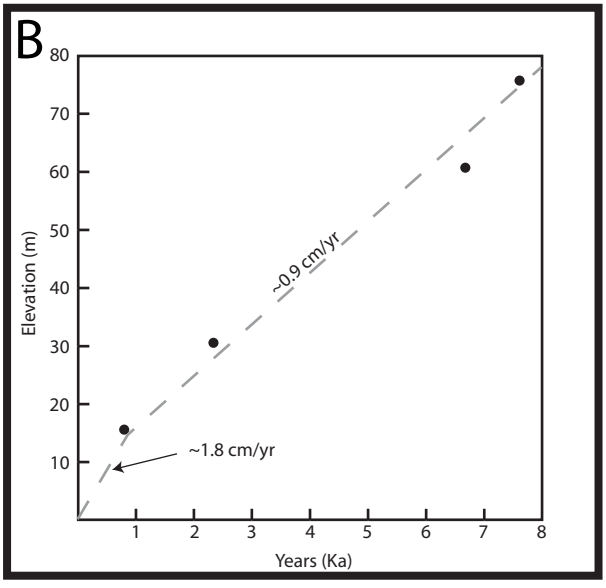
B
Elevation (m)
80
70
60
50
40
30
20
10
~0.9 cm/yr
~1.8 cm/yr
1
2
3
4
5
6
7
8
Years (Ka)

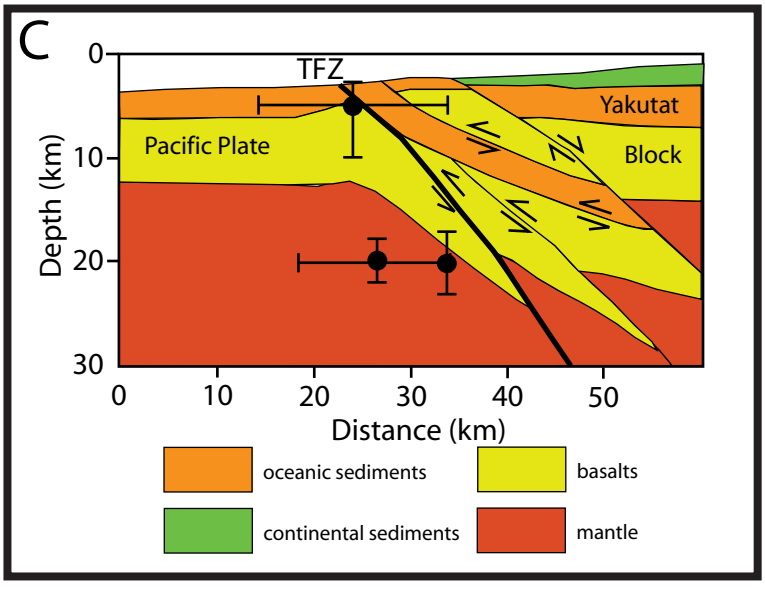
C
0
10
20
30
Depth (km)
TFZ
Yakutat
Block
Pacific Plate
0
10
20
30
40
50
Distance (km)
oceanic sediments
basalts
continental sediments
mantle

2. Tectonic Setting

The Queen Charlotte-Fairweather (QCF) transform extends for over 1000 km from Vancouver Island, British Columbia to the area just north of Yakutat Bay, Alaska (Carlson et al., 1988). The QCF accommodates largely strike-slip motion between the YT and the Pacific and North American plates. However, the North American margin bends to the west near Yakutat Bay and then bends further to the southwest near the Kayak Island Zone, forming a cusp in the plate margin (Figure 1). At this cusp, the collision of the composite YT obscures the transition from strike-slip motion along the QCF to subduction along the Aleutian megathrust, and likely drives deformation as far inland as the central Alaska Range (~500 km). Deformation within and around the perimeter of the YT varies. Offshore, west of the Pamplona Zone, is a highly deformed, broad fold and thrust belt (Figure 2a). Southeast of the Pamplona Zone, the YT remains largely undeformed with only minor folding and faulting (Plafker et al., 1994). Onshore, within the Chugach-St. Elias orogen, deformation is concentrated between the Kayak Island Zone and Yakutat Bay where the Chugach St. Elias fault marks the YT-NA suture and active east-west striking thrusts accommodate convergence (e.g. Pavlis et al., 2004). Along the eastern perimeter of the YT, southeast of Yakutat Bay, where the YT is translated along the Fairweather fault, the degree of convergent deformation associated with the terrane collision is not constrained (Bruhn et al., 2004). Although it is likely that some convergence is accommodated here, the kinematics along this eastern flank of the YT—here called the Fairweather corridor—remain poorly understood.

Deformation of the eastern perimeter of the YT includes a major component of dextral simple shear along the Fairweather fault. The Fairweather fault moves onshore at Icy Point near Glacier Bay and continues onshore for 280 km until ice cover and a complex array of faults obscure its continuation/termination in the St. Elias Mountains. Ongoing activity of the fault was made clear by the M 7.9 1958 Lituya Bay earthquake, which was produced predominantly by dextral faulting and resulted in horizontal and vertical offsets up to 6.5 m and 1 m, respectively (Page, 1969). Rupture during this event was consistent with numerous offset Holocene drainages and geomorphic features, which record an average slip rate of 4.8-5.8 cm/yr over the past 1.3 ka (Plafker et al., 1978).

The lower end of these geologic rates agrees well with modern GPS data, which resolve 45.6 ± 2 mm/yr of slip on the Fairweather fault (Fletcher and Freymueller, 2003). West of the Fairweather fault this rate and its orientation vary little, both in the near (< 5km) and far-field (> 50 km), indicating that the YT moves as a block at an orientation rotated counterclockwise from Pacific plate motion (50.9 ± 1.4 mm/yr at N14.7ºW) (DeMets and Dixon, 1999) (Fletcher and Freymueller, 1999). However, the GPS data in this region are affected by transient strain accumulation at the complex syntaxial bend in the plate boundary as well as the effects of post-glacial rebound, and thus may not accurately represent long-term tectonic motion (Pavlis et al., 2004). Further resolving the degree of obliquity between YT motion and the Fairweather corridor is key in resolving the kinematics of active YT accretion.

Depending on the nature of coupling between the YT and the Pacific plate, a large component of Fairweather fault-normal shortening may need to be accommodated in the Fairweather corridor. The vector of Pacific plate motion relative to North America translates to 48.0 mm/yr of Fairweather fault-parallel (N34ºW) and 16.8 mm/yr of Fairweather fault-perpendicular motion (Figure 2a) (DeMets and Dixon, 1999). GPS and geologic data indicate that the Fairweather fault moves dextrally at nearly the Pacific plate margin parallel velocity and that this motion is transferred northwest and accommodated in the orogenic core and to a lesser extent on the central Denali fault system (Fletcher and Freymueller, 2003; Sauber et al., 1997; Eberhart-Phillips et al., 2002). Additionally, some motion may be transferred westward and accommodated by extrusion or other processes (Pavlis et al., 2004). Where the Fairweather fault-perpendicular component of motion is accommodated is less well constrained. The motion is likely accommodated by a combination of slip on the Transition fault, internal deformation of the Yakutat terrane, and deformation within the Fairweather corridor. Minor active folding in the Yakutat terrane east of the Pamplona Zone suggests that internal deformation is not sufficient to account for a large portion of the 16.8 mm/yr of expected convergence (Plafker et al., 1994). Shallow subduction along the Transition fault, as suggested by Plafker et al. (1994), could account for all of the convergent motion. However, due to its submarine location, even a basic characterization of the Transition fault remains elusive (e.g. Plafker et al., 1994, Pavlis et al., 2004). Convergent

accommodation in the Fairweather corridor is also largely unknown, but likely trades off with slip on the Transition fault. Portions of the Transition fault are overlain by up to 800 m of undeformed sediments, and, although these sediments do not preclude recent motion on the Transition fault (Pavlis et al., 2004), they indicate that some convergence is likely transferred to the Fairweather corridor.

One way to estimate convergent deformation within the Fairweather corridor is to constrain surface uplift. Active surface uplift rates derived from GPS as well as tide gauge data indicate that the Fairweather corridor is uplifting at some of the fastest rates on Earth, with peak rates > 3 cm/yr (Larsen et al., 2003; 2004; 2005). These short-term rates are largely attributed to postglacial rebound, and the long-term tectonic component of surface uplift has not been resolved. Models driven entirely by deglaciation can reproduce the observed uplift (Larsen et al., 2004); however, extreme coseismic uplift (14 m) in Disenchantment Bay and the broad arching of Yakutat Bay and Russell Fjord during the 1899 Yakutat Bay earthquake indicate that at least some component of the active uplift is tectonic (Tarr and Martin, 1912; Plafker and Thatcher, 1982). Dated marine terraces in Lituya Bay record steady uplift rates of ~1 cm/yr over the past 7 ka (Figure 2b) (Hudson el al., 1976), implying that a component of uplift was active prior to recent deglaciation and further indicating that a component of recent surface uplift is tectonically driven. Time-averaged Holocene sedimentation rates between Icy Bay and Cross Sound (Figure 2) of 7.9 mm/yr, corresponding to a rough region-wide erosion rate of 5.1 mm/yr (Sheaf et al., 2003), suggest that bedrock uplift has been active throughout the Holocene. Additionally, when GPS data is corrected for shear strain along the Fairweather fault, and for horizontal motions driven by glacial rebound, a residual 3-5 mm/yr of convergence is resolved along the Fairweather corridor (although this is an uncertain estimate requiring many assumptions) (Larsen; pers. comm., 2006). Thus, most evidence indicates recent tectonic uplift in the Fairweather corridor. Understanding the relationship between this recent tectonic uplift and the long-term uplift that has built the Fairweather Range requires additional information.

If mountain building has been active in the past few million years along the Fairweather corridor, it should be reflected in the character of topography. The Fairweather and Southern Icefield Ranges (Figure 3) lie to the east of the Fairweather

fault and rise from sea level to exceed 4 km in elevation (e.g. Mt. Fairweather, 4,665 m) over as short as 20 km, creating spectacular coastal relief (Figure 4). High peaks are concentrated in two areas: near Mt. Vancouver north of Yakutat Bay, and 200 km to the south at the northern reaches of Glacier Bay, where Mt. Fairweather is located. Between these two areas, in the zone surrounding the Alsek River, peak heights are significantly lower and rarely exceed 2500 m (Figure 5 AA'; Figure 6). Mean elevation in a narrow swath directly east of the Fairweather fault shows a similar trend, reaching a maximum (~2000 m) in the Mt. Vancouver and Mt. Fairweather regions, and decreasing in the intervening Alsek River region (Figure 7, swath 2 and 3). However, when mean elevation is calculated for a 150 km zone east of the Fairweather fault, a different north-south pattern emerges. The zone surrounding Mt. Vancouver has the highest mean elevation (~1800 m); however, south of Mt. Vancouver, mean elevation only deviates slightly and is, on average, 1000 m—even in the high peak region near Mt. Fairweather (Figure 6). This indicates that the zone of high mean elevation is more laterally extensive in the orogen proximal Mt. Vancouver region than in the more removed Mt. Fairweather region. Changes in elevation across the corridor, normal to the Fairweather fault, are variable. Near Mt. Vancouver, mean elevation increases as the Fairweather fault and orogenic core are approached (i.e. elevations on swath 2 and 3 are higher than on 5 and 6; Figure 7). In the Alsek River region, mean elevation does not vary systematically with distance from the Fairweather fault. Near Mt. Fairweather, high mean elevation is concentrated in narrow zone directly adjacent to the fault which extends along strike for ~100 km (Figure 5, AA', DD', EE'). The topographic form of this region is striking in comparison to the chaotic elevation trends in the Alsek River region. Maximum slopes throughout the Fairweather corridor are high (65-75º) (Figure 8, 9). Average slopes are more moderate and are consistently around 14º to the east of the Fairweather fault (150 km swath), with only minor deviations along strike (Figure 9). However, narrow strike profiles indicate that the areas surrounding the high topography regions of Mt. Vancouver and Mt. Fairweather differ in average slope, with the Mt. Fairweather region having a higher average slope (25º vs. 18º) (Figure 10).

Topography to the west of the Fairweather fault also varies from north to south. North of the Alsek River are two geomorphic domains—a low elevation, low-relief

coastal plain and the rugged ~30-km-wide Yakutat foothills (mean elevation ~500 m), which rise above the coastal plain on a linear, 100-km-long, 500-m-high, escarpment (Figure 5, BB'). South of the Alsek River, a coastal plain is absent and the Fairweather fault is bounded on the west by a narrow belt of rugged topography. Taken together, the rugged topography, high elevation, and linear escarpment in the Fairweather corridor are strong evidence for both convergence and recent rock uplift. However, the localized geometry and higher average slope of the high elevation Mt. Fairweather region relative to the orogen proximal Mt Vancouver region, suggest that topography building processes in the Fairweather corridor are different than those in the orogenic core.

If a significant degree of long-term bedrock uplift has occurred in the Fairweather corridor, this may be reflected in the recent exhumation history, provided the region is approaching topographic steady-state. Exhumation can be constrained using time-temperature data derived from low-temperature thermochronology. Reconnaissance apatite fission-track dating was conducted by O'Sullivan et al. (1997) in the region north of the Alsek River. Thirteen apatite-fission track ages (AFT) in the region are as young as 1.3 Ma and average 2.8 Ma (excluding one anomalous age of 9.5 Ma), indicating rapid Plio-Pleistocene cooling. Based on a diffuse age-elevation trend, O'Sullivan et al. (1997) suggested a poorly constrained regional exhumation rate of 1.5-1.9 mm/yr. Additionally, O'Sullivan et al. (1997) noted no obvious changes in cooling history with distance from either the orogenic core of the St. Elias Mountains or active or inactive structures, which suggests broad regional denudation. These preliminary data suggest that the entire region is a zone of rapid, recent exhumation. However, both the sparse sample coverage north of the Alsek River and the lack of samples along the southern portion of the Fairweather fault preclude analysis of the role of the entire Fairweather corridor in the long-term regional kinematics. New data are needed to further resolve patterns and rates of exhumation in the Fairweather corridor and to constrain its role in active orogenesis.

Figure Captions

Figure 3: Shaded relief map of the Fairweather corridor, including parts of Alaska and northern Canada. Elevation data from the Geological Society of Canada (GSC) and USGS were used and are available online.

Figure 4: *a)* Aerial photograph showing the rugged topography and glacial coverage in the area near Mt. Fairweather. *b)* Photograph of Johns Hopkins Inlet exhibiting the extreme relief of the Fairweather Range. Photographs were taken during the 05' summer field season.

Figure 5: Topographic profiles derived from 1 arc second National Elevation Data (NED). Profiles locations shown in Figures 3 and 13. Major landforms and structures along the profiles are indicated; FF-Fairweather fault; BRFS-Border Ranges fault system. Dotted arches highlight the topographic form of the Mt. Fairweather region (see text).

Figure 6: Along strike trend in mean and maximum elevation for the 150-wide-zone east of the Fairweather fault (Figure 8, swaths 2-6). Values of mean and maximum elevation are recorded in 10 x 150 km cells. Note the difference in mean elevation between the two zones with high peaks.

Figure 7: Along strike trend in mean elevation for each 30-km-wide swath shown in Figure 8. Swath 1 provides elevations west of the Fairweather fault. South of 200 km large portions of this swath lie in the Pacific Ocean. Swaths 2 and 3 are in bold to highlight patterns directly east of the Fairweather fault.

Figure 8: Slope map derived (using ArcGIS) from data available at USGS and GSC websites. The white box represents the 180 x 360 km zone analyzed in all topographic analyses (Figures 6-9). The analyzed zone was broken into a grid of 10 x 30 km blocks, forming six Fairweather fault-parallel, 30-km-wide swaths.

Figure 9: Along strike trend in mean and maximum slope for the 150-wide-zone east of the Fairweather fault (swaths 2-6). Values are recorded for 10 x 150 km cells.

Figure 10: Along strike trend in mean elevation for each 30-km-wide swath. Note the steep slopes in the Mt. Fairweather region adjacent to the Fairweather fault.

Figure 3

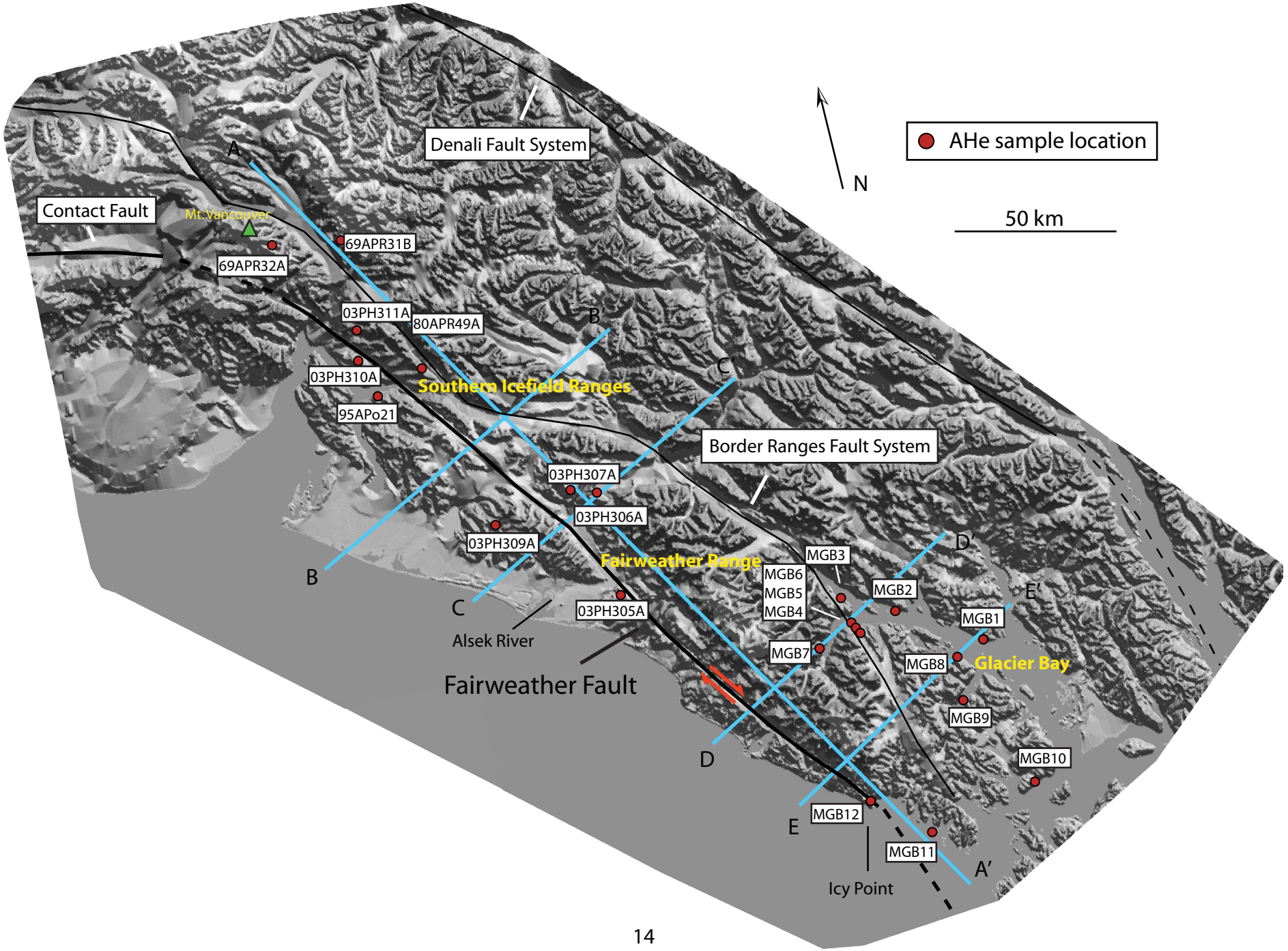
Denali Fault System
Contact Fault
Mt. Vancouver
69APR31B
69APR32A
03PH311A
80APR49A
03PH310A
95APo21
Southern Icefield Ranges
Border Ranges Fault System
03PH307A
03PH306A
03PH309A
Fairweather Range
03PH305A
Alsek River
Fairweather Fault
MGB3
MGB6
MGB5
MGB4
MGB2
MGB1
MGB7
MGB8
Glacier Bay
MGB9
MGB10
MGB12
MGB11
Icy Point
A
A′
B
B′
C
C′
D
D′
E
E′
N
AHe sample location
50 km

Figure 4

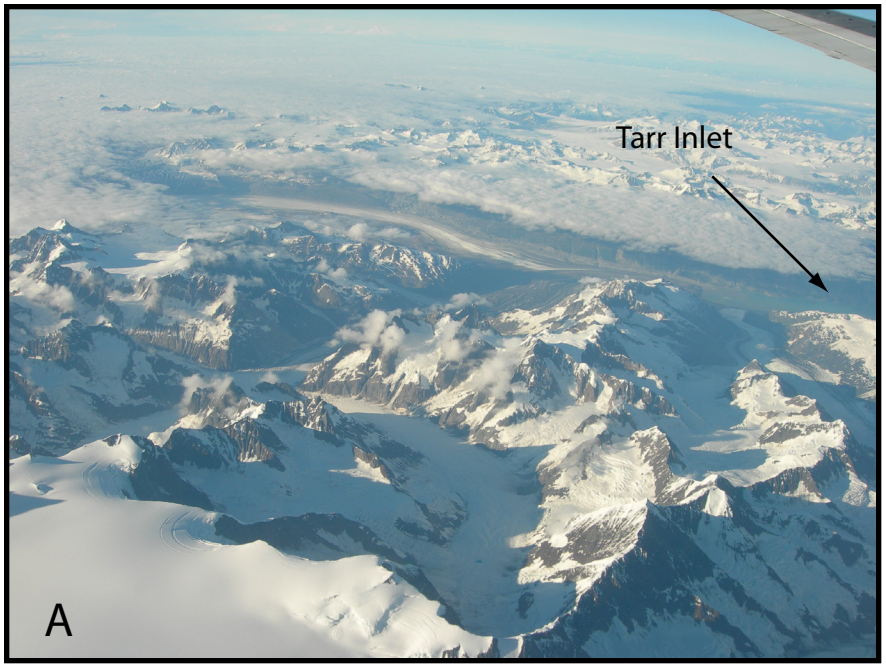

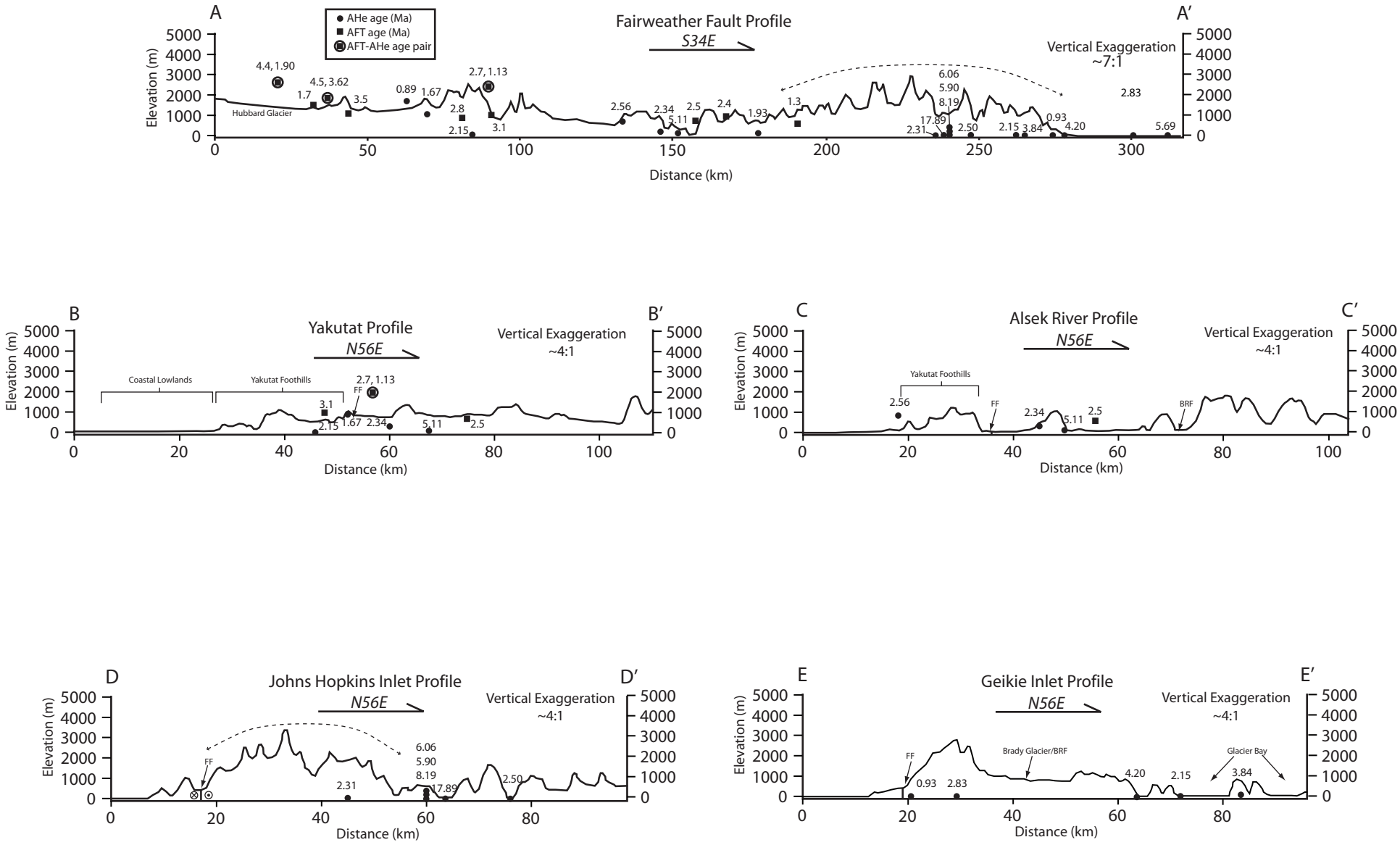
A
A′
AHe age (Ma)
AFT age (Ma)
AFT-AHe age pair
Fairweather Fault Profile
S34E
Vertical Exaggeration
~7:1
Elevation (m)
Distance (km)
Hubbard Glacier
4.4, 1.90
4.5, 3.62
1.7
3.5
0.89
1.67
2.7, 1.13
2.8
2.15
3.1
2.56
2.34
5.11
2.5
2.4
1.93
1.3
6.06
5.90
8.19
17.89
2.31
2.50
2.15
3.84
0.93
4.20
2.83
5.69
B
B′
Yakutat Profile
N56E
Vertical Exaggeration
~4:1
Coastal Lowlands
Yakutat Foothills
FF
2.7, 1.13
3.1
2.15
1.67
2.34
5.11
2.5
C
C′
Alsek River Profile
N56E
Vertical Exaggeration
~4:1
Yakutat Foothills
2.56
FF
2.34
5.11
2.5
BRF
D
D′
Johns Hopkins Inlet Profile
N56E
Vertical Exaggeration
~4:1
FF
6.06
5.90
8.19
2.31
17.89
2.50
E
E′
Geikie Inlet Profile
N56E
Vertical Exaggeration
~4:1
FF
Brady Glacier/BRF
Glacier Bay
0.93
2.83
4.20
2.15
3.84

Figure 5

Figure 6

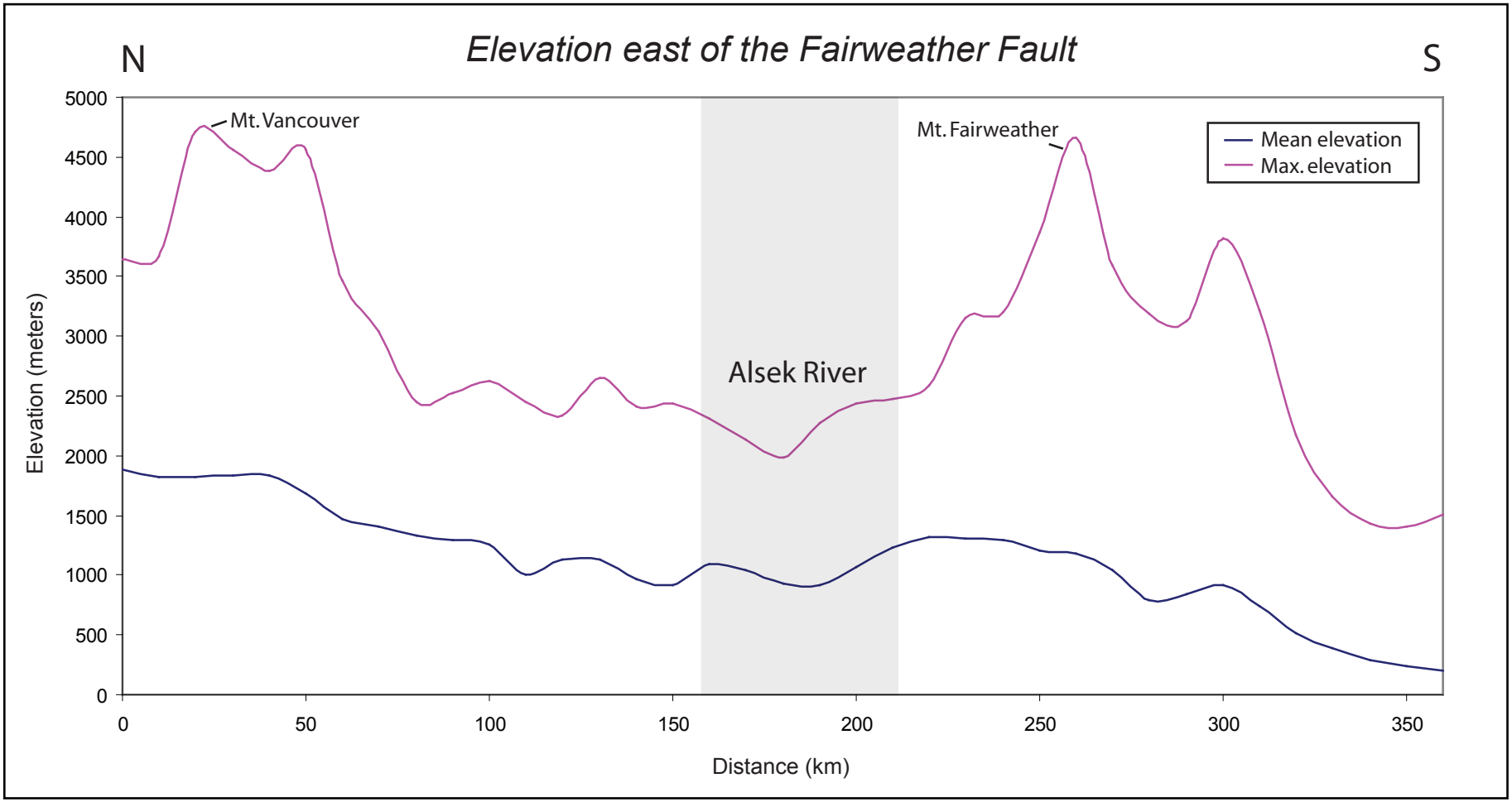
N
Elevation east of the Fairweather Fault
S
Mt. Vancouver
Mt. Fairweather
Mean elevation
Max. elevation
Alsek River
Elevation (meters)
5000
4500
4000
3500
3000
2500
2000
1500
1000
500
0
0
50
100
150
200
250
300
350
Distance (km)

Figure 7

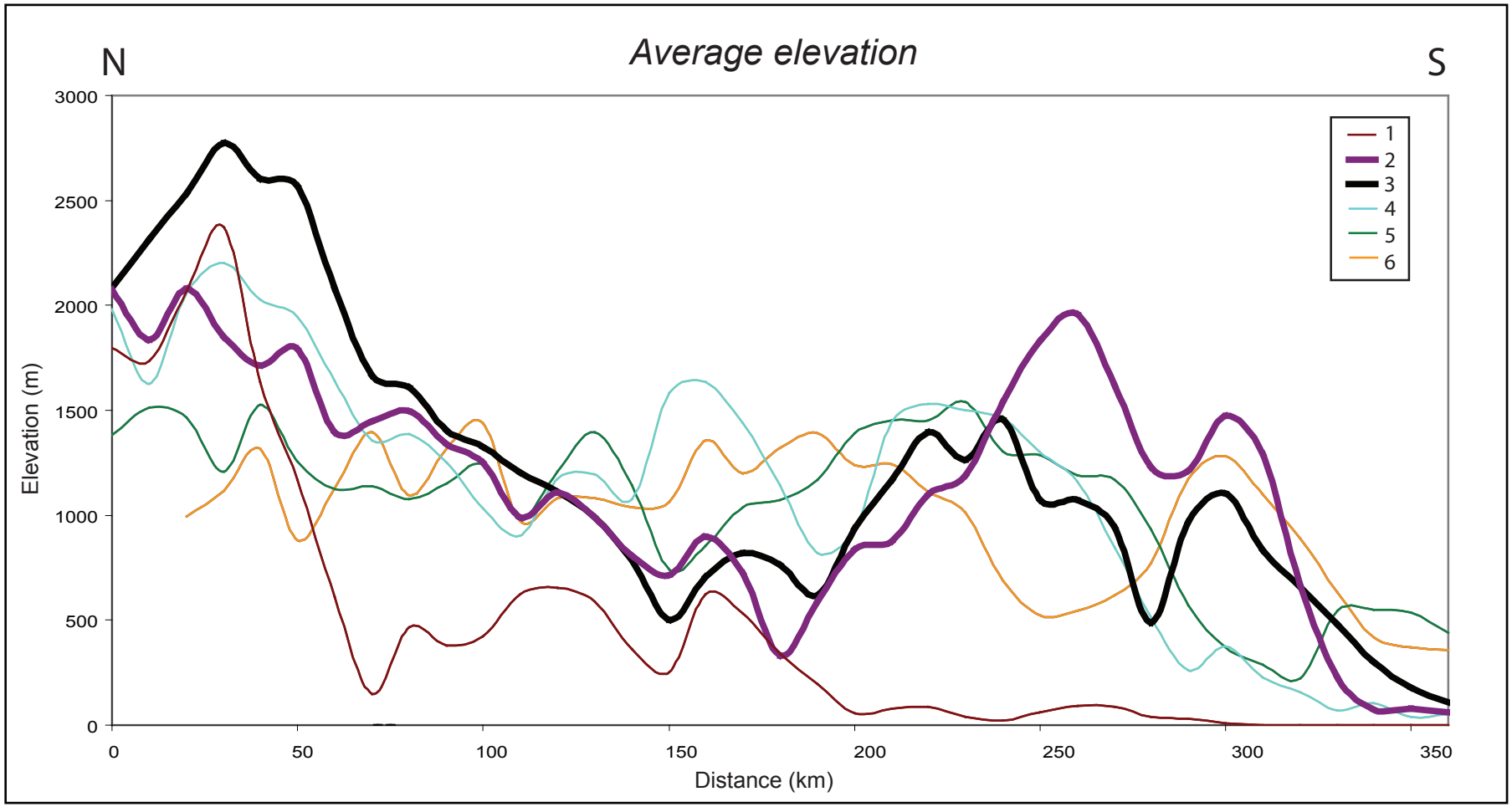
N
Average elevation
S
3000
2500
2000
1500
1000
500
0
Elevation (m)
0
50
100
150
200
250
300
350
Distance (km)
1
2
3
4
5
6

Figure 8

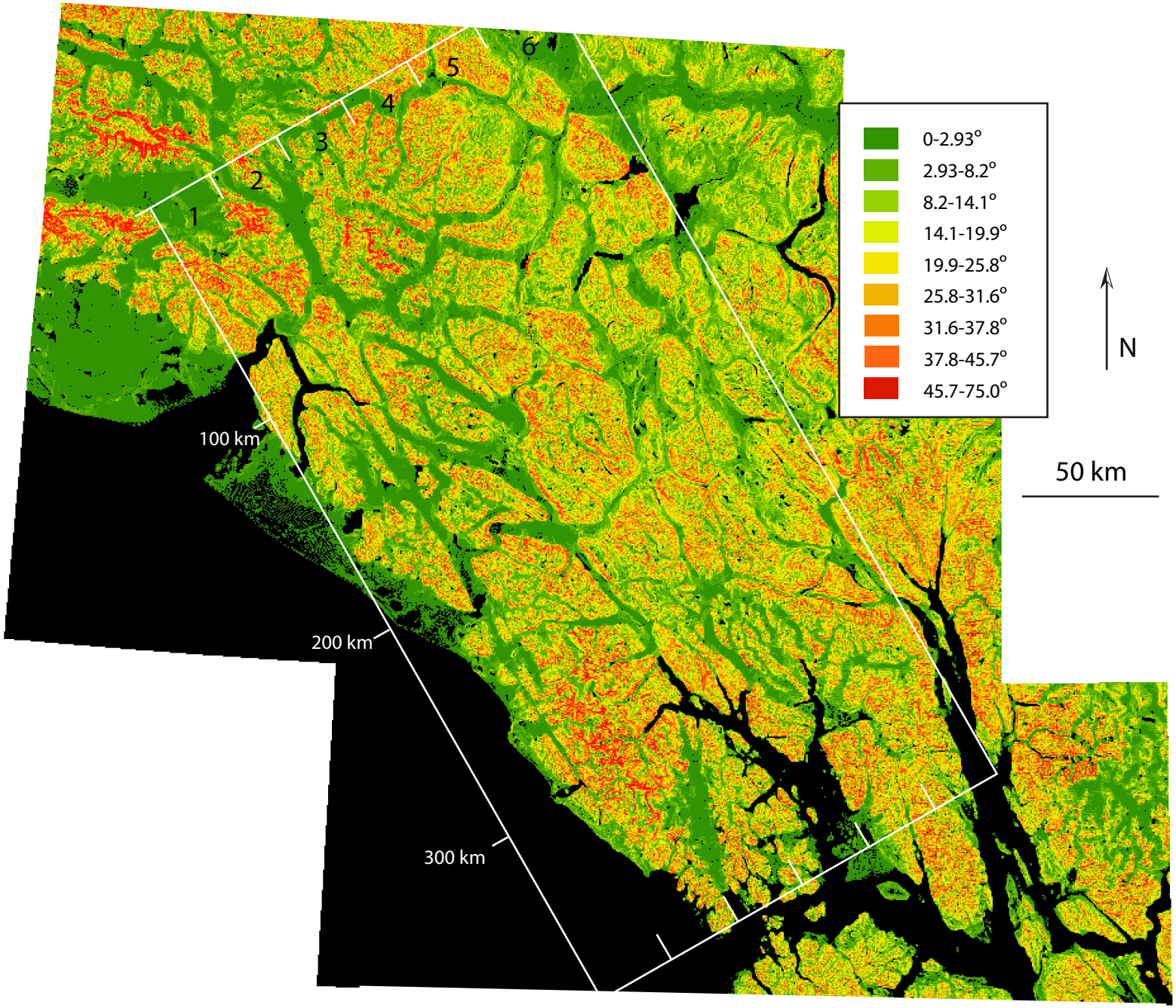
1
2
3
4
5
6
100 km
200 km
300 km
0-2.93°
2.93-8.2°
8.2-14.1°
14.1-19.9°
19.9-25.8°
25.8-31.6°
31.6-37.8°
37.8-45.7°
45.7-75.0°
N
50 km

Figure 9

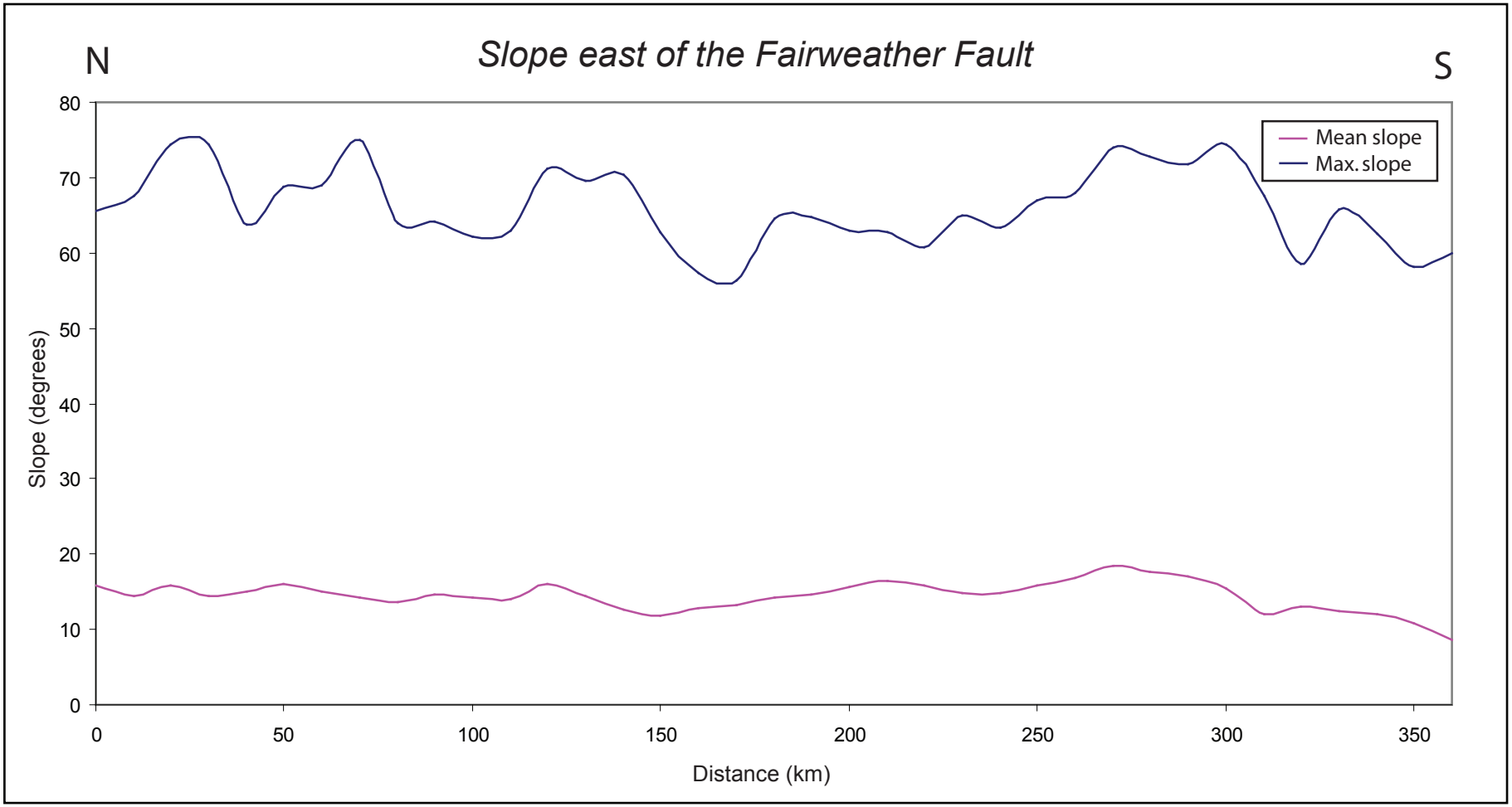
N
Slope east of the Fairweather Fault
S
Mean slope
Max. slope
Slope (degrees)
0
10
20
30
40
50
60
70
80
0
50
100
150
200
250
300
350
Distance (km)

Figure 10

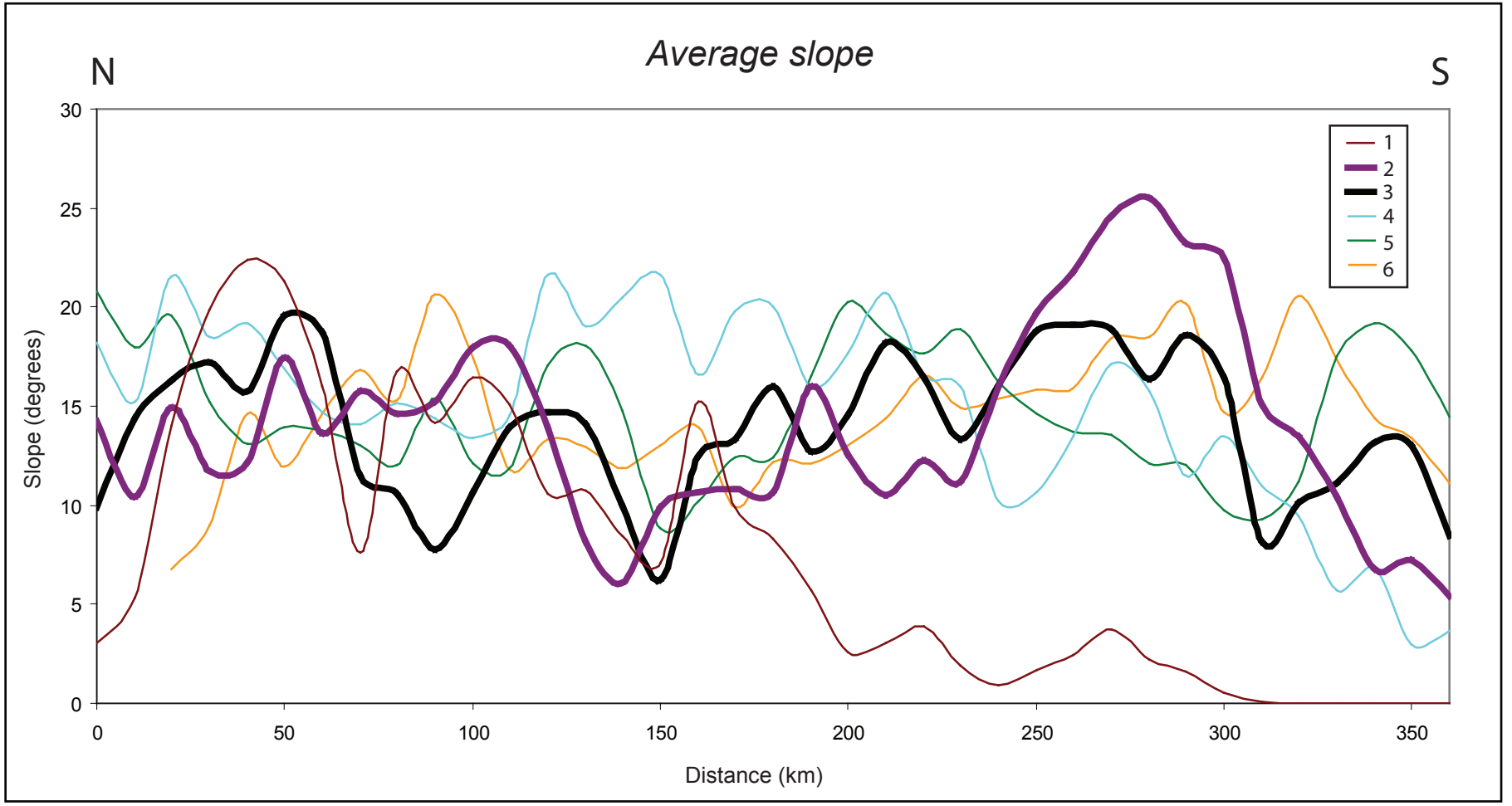
Average slope
N
S
Slope (degrees)
30
25
20
15
10
5
0
0
50
100
150
200
250
300
350
Distance (km)
1
2
3
4
5
6

3. Methods

3.1 Low Temperature Thermochronology and U-Th/He dating

Traditional geomorphology uses field observations to examine the history and evolution of landscapes. As a result, quantification of landscape evolution has been limited to areas where the evidence of landscape process has not yet been removed by erosion. Thus, geomorphology has been temporally limited in scope. However, some of these constraints have recently been alleviated with the advent of low temperature thermochronology, whereby rates of overburden removal (~erosion) can be estimated from cooling rates determined by temperature-sensitive processes in minerals (Dodson, 1973). And so, rock currently at the Earth's surface can be used to provide a quantitative analysis of the removal rate of previous overburden. This tool greatly expands the temporal scope of geomorphology, and offers quantitative insight into the processes that build and denude mountain belts.

One mineral system that has long been recognized as a potential chronometer is the (U-Th)/He system (e.g. Strutt, 1908). The basis of this system is that ^{4}He, or alpha particles, accumulate at a known rate from the decay of ^{238}U, ^{235}U, ^{232}Th, and to a lesser extent (generally negligible) ^{147}Sm. The cumulative age equation for these decay chains is (ignoring Sm):

$$^{4}He = 8^{238}U(e^{\lambda_{238}t} - 1) + 7(^{238}U/137.88)(e^{\lambda_{235}t} - 1) + 6^{232}Th(e^{\lambda_{232}t} - 1) \qquad \text{(eqn. 1)}$$

where ^{4}He, ^{238}U, ^{232}Th are the present day measured amounts of each isotope, λ is the decay constant for each isotope, and t is the apatite cooling age (AHe). The constants preceding the U and Th abundances represent the number of alpha particles emitted in each decay chain, while 1/137.88 is the present day ratio of ^{235}U/^{238}U (Farley, 2002).

Despite the well characterized decay chains of the above isotopes, initial attempts at using the apatite (U-Th)/He system to date crystallization consistently produced ages younger than those determined from other techniques (Reiners et al., 2005). The curiously young ages were attributed to the poor retention of ^{4}He under geologic conditions, and for this reason apatite (U-Th)/He (AHe) crystallization age dating was largely abandoned. However, the systematically young ages recorded by the AHe system

suggested that the AHe "apparent age" may instead represent the age since the mineral cooled from low temperatures (Zeitler et al., 1987).

Laboratory step-heating diffusion studies showed that helium diffusion from apatite was well characterized as a thermally activated process (e.g. Zeitler et al., 1987, Wolf et al., 1996). Thus, a closure temperature (T_c)—the temperature at the time corresponding to the apparent age recorded by the AHe system—could be derived (Dodson, 1973). Further studies showed that for typical crustal cooling rates of 10°C/Ma and grain radii of 50-150 μm, the T_c for AHe was 63-73°C (Figure 11a) (Farley, 2000). This T_c corresponds to crustal depths of ~2-4 km for typical continental geothermal gradients. Thus, the AHe system records the last stages of the cooling during exhumation. In many instances this cooling is driven by removal of overburden by surface processes, which is why AHe dating is a powerful tool in the study of landscape evolution.

3.2 Analytical Procedures

Rock samples (3-8 kg) were processed using standard crushing and mineral separation techniques at Virginia Tech. The apatite separate was then examined and aliquots of apatite were selected and placed into 0.7 x 1 mm Platinum tubes and the ends were sealed. The tubes were then placed inside larger 1.5 x 2 mm Platinum tubes, which were sealed and labeled for identification post-He extraction. Groups of 8 tubes were loaded into a copper track and sequentially dropped into a boron nitride cup located inside a resistively-heated ultra high vacuum furnace. The furnace was heated to >940°C for 20 minutes to drive off all accumulated helium within the apatite crystals. Helium was then purified from the evolved gas in a cryogenic trap cycling between 16-37 K. The remaining gas was combined with a ^{3}He spike and sent through a quadrupole mass spectrometer where the ^{4}He/^{3}He ratio was measured and the outgassed ^{4}He was calculated. Next, the large Pt tubes were opened under microscope. The smaller tubes were removed, placed in teflon vials, and opened under ~150 μL of ultra-pure distilled water. The grains were then dissolved in HNO_3 and spiked with known amounts of ^{235}U and ^{230}Th. The resulting solution was then shipped to either Yale University or Caltech,

where the U and Th concentrations were measured by isotope dilution using inductively coupled plasma mass spectrometry (ICP-MS).

The AHe closure temperature is affected by grain size. Thus, prior to the loading of apatite aliquots, the grain size and approximate grain geometries were measured. Grain size is directly incorporated into the following bulk closure temperature equation for thermally activated diffusion (McDougall and Harrison, 1999):

$$T_c = \frac{E/R}{\ln\left[\frac{ART_c^2 D_0/a^2}{EdT/dt}\right]} \qquad \text{(eqn. 2)}$$

where T_c is the closure temperature, E is the activation energy (33 kcal/mol) (Farley, 2000), R is the gas constant, A is a shape factor (55 for an infinite cylinder) (Dodson, 1973), D_0 is the diffusivity at infinite temperature (50 cm^2/s) (Farley, 2000), dT/dt is the cooling rate, and *a* is the diffusion domain radius. In apatite, the diffusion domain is the grain itself (Farley, 2000), meaning that the measured grain radius is *a* in equation 2. Aliquots were picked to have grains of similar radii, and the mass weighted average radius (MWAR) was used to calculate the T_c by solving equation 2 iteratively. Aliquot Tc's were averaged in order to calculate cooling rates for each sample.

Additionally, the AHe age itself is affected by grain size. The energy of alpha decay moves alphas ~20 μm through the apatite crystal lattice before the kinetic energy is dissipated (Farley et al., 1996). Thus, ^{4}He generated after apatite has cooled below its closure temperature may still be lost at grain edges, resulting in erroneously young cooling ages (Figure 11b). A correction for the alpha ejection was developed using analytical solutions and Monte Carlo modeling (Farley et al., 1996). Alpha ejection was shown to be dependent on the grain's surface area to volume ratio (β) by the equation:

$$F_T = 1 - 4.695\beta + 3.381\beta^2 \qquad \text{(eqn. 3)}$$

The measured age can then be divided by the value of F_T to get a corrected AHe age. Apatite crystals were treated as flat ended hexagonal prisms, and β was calculated for each grain based on length and width measurements made at 110X magnification. The F_T was then calculated by summing the mass weighted contribution of each grain. The F_T was then applied to AHe age calculated from the ^{4}He and ^{235,238}U, ^{232}Th values.

Apatite grains were examined for birefringent inclusions under cross polars at 110X using an Olympus binocular scope. Apatite grains often contain inclusions of other minerals with high U and Th concentrations, such as zircon, monazite, and xenotime (e.g. Ehlers and Farley, 2003). These different minerals result in zones of higher helium concentration, which affect helium gradients and alter diffusion rates. Concentrated helium zones also affect the accuracy of the F_T correction. Additionally, the methods used to dissolve the apatite for ICP-MS analysis do not dissolve zircon. Therefore, the helium contributed by the zircon inclusion will be measured, but the U and Th will not, resulting in anomalously old AHe ages. In most cases, only inclusionless, pristine grains with the best geometries were loaded for age determination. In some cases, however, due to poor apatite quality, grains with low birefringence inclusions were loaded. Additionally, when possible, large grains were chosen to minimize the F_T correction—only in rare cases did samples have F_T corrections less than 0.70. To assess the potential effect of random inclusions, multiple (3 or more) aliquots were measured for most samples.

Age uncertainties are estimated by analysis of standards and reproducibility of multiple aliquots from individual samples. We report age errors of 10% (2σ) based on the reproducibility of Durango fluorapatite and other standards at Virginia Tech. However, in some cases individual samples reproduced poorly (2σ > 10%) in which case the standard deviation of replicate analysis was reported. An additional age uncertainty due to helium blank correction was applied to samples with total gas content < 0.001 pmol, at which point the uncertainty in blank corrections is > 10% (2σ). All sample ages except those clearly affected by instrumentation error are included in Table 1. In some cases single ages differ significantly from other aliquots for the same sample. These outliers are included in the Table 1, but are not included in sample averages used to interpret ages.

3.3 Sampling strategy

The main objective of this study was to understand the temporal and spatial pattern of exhumation in the Fairweather corridor. Specific goals included sampling both along and across the strike of the plate bounding active structure, the Fairweather fault,

and collecting an age-elevation transect. However, funding limitations and the rugged and remote nature of the Fairweather Range greatly reduced the number of accessible localities. To combat some of these problems, existing samples from higher temperature studies in the northern Fairweather Range were utilized, based on sample material provided by T. Pavlis, P. Haeussler, and P. O'Sullivan from previous studies. Twelve samples were chosen from previous work to provide the best spatial coverage possible and to represent lithologies conducive to AHe dating (e.g. granitic rock) (Figure 3). These rocks form an along strike transect from Mt. Vancouver, ~30 km north of the last mapped trace of the Fairweather fault, to the Alsek River area some 150 km along-strike to the southeast. The samples also provide coverage in a broad zone surrounding the fault, with 3 samples forming an ~30 km fault-perpendicular transect.

In addition, twelve rock samples were collected in Glacier Bay National Park and Preserve (GBNP) in the summer of 2005. These samples provide an additional 150 km of along-strike sampling and complete a sampling of the entire onshore trace of the Fairweather fault at 30-50 km spacing (Figure 3). The GBNP samples also provide data at distances up to 60 km from the fault. These samples are important for assessing the extent of rapid exhumation both in relation to the Fairweather fault and the St. Elias orogenic core. The samples were collected by boat and sea kayak, and thus were largely limited to sea level localities in the fjords of Glacier Bay and along the Pacific coast.
Although an elevation transect of ~220 m was collected along Mt. Parker in GBNP, rugged terrain, and time and monetary constraints prohibited the collection of a large relief elevation transect. Also, existing samples in the northern Fairweather Range, although highly variable in elevation, did not provide a spatially narrow elevation transect. Therefore, the temporal variance in cooling rates could not be examined using an age-elevation relationship for AHe ages. To partially circumvent this limitation, the mineral-pair technique (AHe, AFT) was used to examine changing cooling rates.

The mineral-pair technique uses ages that are determined from different closure temperatures in order to evaluate temporal changes in exhumation rate (Figure 12a) (e.g. Kirby et al., 2002). In contrast, age-elevation transects use multiple samples and a single technique to examine variation in exhumation rates (Figure 12c) (e.g. Fitzgerald et al., 1995). One advantage of the age-elevation technique is that it has the potential to reveal

a partial retention zone (PRZ)—a zone over which thermally controlled helium diffusion is partial (Figure 11a) (Ehlers and Farley, 2003). The helium PRZ for apatite is known to be ~40-80°C; thus, if the PRZ can be bracketed between sample elevations, the paleogeothermal gradient can be constrained (e.g. Stockli et al., 2000). This paleogradient estimation is important for the conversion of cooling rates to exhumation rates. However, in active areas approaching topographic steady state (Willett and Brandon, 2002), as may be expected in southern Alaska where high relief and heavy precipitation lead to rapid erosion, exhumation of a helium PRZ is unlikely over accessible elevation ranges. More commonly active mountain belts near steady-state have nearly age-invariant elevation transects (e.g. House et al., 2002, Searle, 1997), due to a combination of rapid exhumation and a high admittance ratio (ratio of isotherm relief to topographic relief (Reiners et al., 2003)). Thus, the mineral-pair method, in addition to being logistically more practical than an age-elevation transect, may also contain more exhumational information (Spotila, 2005).

Figure Captions

Figure 11 a) Schematic showing AHe and zircon (U-Th)/ He (ZHe) closure temperatures (Tc) and partial retention zones (PRZ). For the conditions shown Helium retention in the AHe system is complete (100%) at lower than 40° C, and partial from 40-80° C, resulting in an effective closure temperature of 70° C (for ZHe; PRZ = 195-160° C, Tc =180° C). At point A in the schematic borehole no He is lost from apatite by volume diffusion. An AHe age from a sample collected at this depth would represent the time it took for the crystal to cool from 70-20° C due to rock uplift. At point B a portion of the produced He is retained in the apatite crystal and a portion is lost due (partial retention). The AHe age will be > 0 despite being above the Tc. At point C all He produced by α-decay in apatite is lost. A sample removed from this depth would have an AHe age of zero. Similar concepts apply for ZHe ages of the borehole samples. b) Representation of the effect of alpha-ejection. The energetics of alpha-decay move He atoms ~ 20 μm through the crystal lattice (Farley et al., 1996). If the He-producing atom is within 20 μm of the grain edge, there is a finite chance the He atoms will be lost. Alpha ejection results in He loss even after the system is closed in regards to volume diffusion.

Figure 12 a) The mineral-pair method uses different closure temperatures to infer the time-temperature (t-T) path of a single rock. b) If the thermal field in the crust is invariant cooling rates can be obtained by interpolating between (t, T) points derived from each thermochronometric age. c) Vertical relief transects use a single thermochronometer to obtain exhumation rates from time-elevation (t-Z) data from multiple samples. d) If the closure isotherm is flat over the span of the transect the difference in elevation between samples can be divided by the age difference to define an exhumation rate.

Figure 11

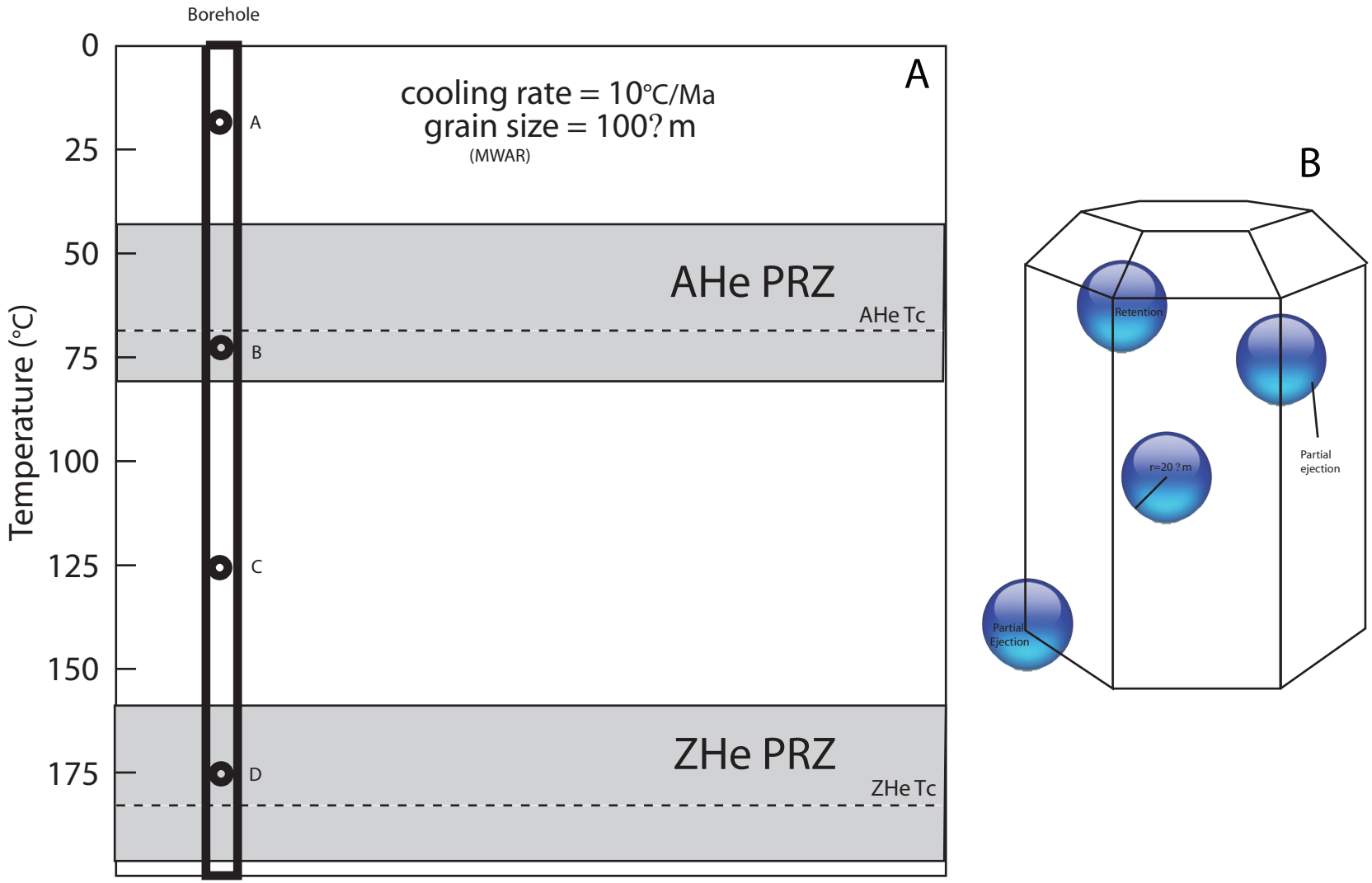
Borehole
0
25
50
75
100
125
150
175
Temperature (°C)
A
cooling rate = 10°C/Ma
grain size = 100? m
(MWAR)
AHe PRZ
AHe Tc
ZHe PRZ
ZHe Tc
A
B
C
D
B
Retention
Partial ejection
r=20 ? m
Partial Ejection

Figure 12

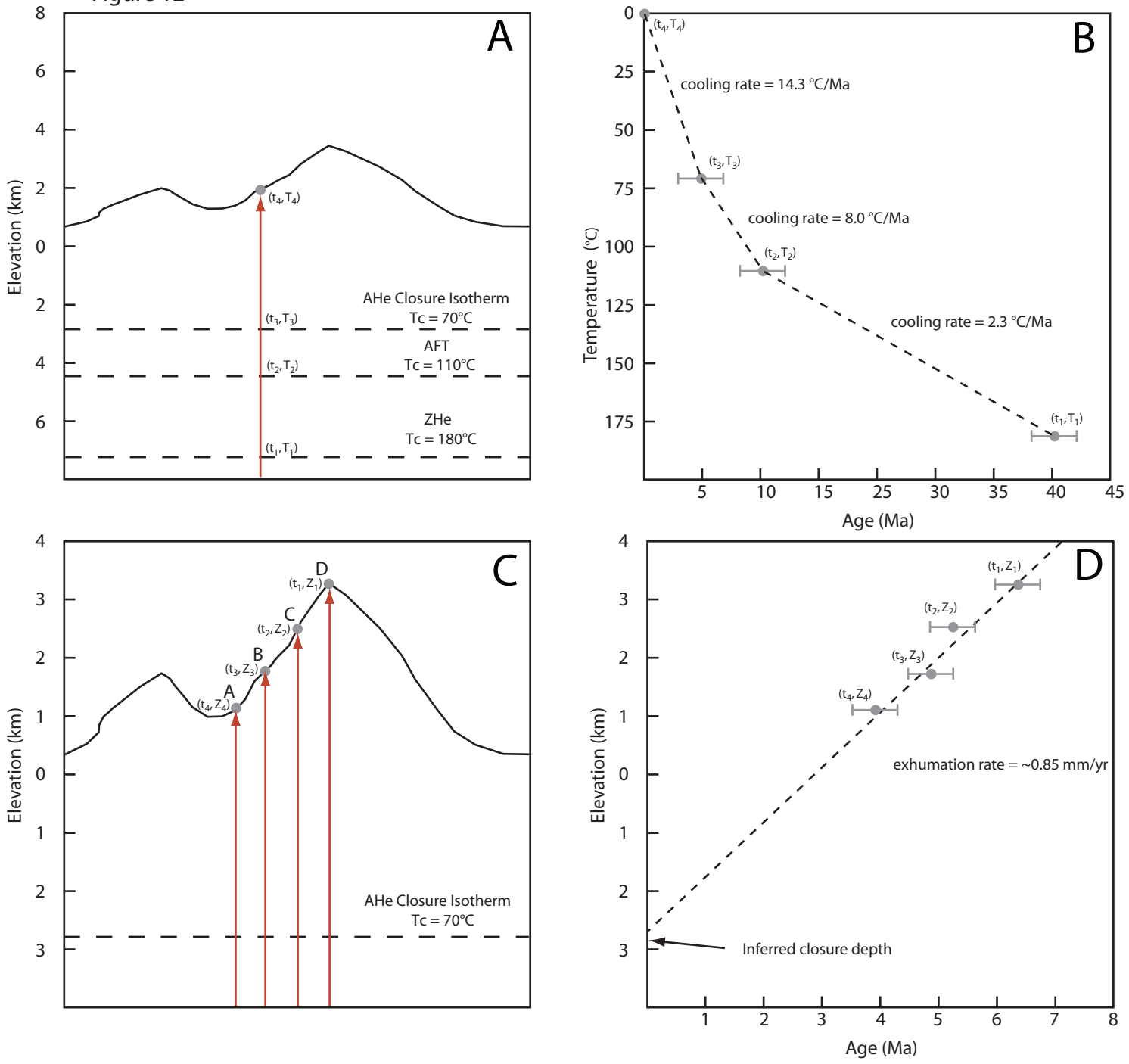
A
Elevation (km)
(t4, T4)
(t3, T3)
(t2, T2)
(t1, T1)
AHe Closure Isotherm
Tc = 70°C
AFT
Tc = 110°C
ZHe
Tc = 180°C
B
Temperature (°C)
cooling rate = 14.3 °C/Ma
cooling rate = 8.0 °C/Ma
cooling rate = 2.3 °C/Ma
Age (Ma)
C
A
B
C
D
(t4, Z4)
(t3, Z3)
(t2, Z2)
(t1, Z1)
AHe Closure Isotherm
Tc = 70°C
D
exhumation rate = ~0.85 mm/yr
Inferred closure depth
Age (Ma)

4. **Results**

Average sample ages range from 17.9 to 0.89 Ma, and 16 of 22 ages fall between 2 and 5 Ma (Table 1) (Figure 13). Young ages (< 3 Ma) are not restricted to areas close to the core of the St. Elias orogen, rather they are found as far as 280 km south along the trace of the fault (Figure 14). Additionally, young ages are not limited to a narrow zone surrounding the Fairweather fault. Sample ages < 3 Ma are found at distances greater than 50 km from the fault trace (Figure 15). These data indicate that Plio-Pleistocene cooling has occurred in a broad zone encompassing much of the Fairweather corridor.

Samples north of the Alsek River range from 0.89 to 5.11 Ma with an average sample age of 2.32 Ma (Table 1, Figure 13). The youngest AHe ages occur near Yakutat Bay (0.89-1.67 Ma), indicating a zone of extremely rapid cooling near the orogenic core and the terminus of the Fairweather fault (Figure 16). Similar to O'Sullivan et al. (1997), there is no obvious trend relative to structural boundaries. However, the two oldest AHe ages north of the Alsek River (3.62, 5.11 Ma) are from the samples at the greatest distance from the Fairweather fault, suggesting exhumation increases towards the fault trace. AHe cooling ages exhibit no correlation with elevation (Figure 17). A temporal relationship between AHe and O'Sullivan et al's (1997) AFT ages is also unclear. Single sample AFT-AHe paired ages record variable changes in cooling rate, with two samples indicating an increased cooling rate since the Pliocene, and one indicating a rate decrease (Figure 18).

In GBNP, samples exhibit a much greater age range (2.15-17.9 Ma), but most ages fall between 2 and 6 Ma. These ages are similar to those North of the Alsek River, and indicate rapid cooling in the Fairweather corridor extends as far south as Cross Sound (Figure 13). Ages exhibit no clear variation with distance from the Fairweather fault or across structural boundaries. The youngest AHe age is from Icy Point, within meters of the Fairweather fault, suggesting recent rapid cooling near the fault. However, this sample produced low quality apatite and exhibited poor age reproducibility (MGB12, Table 1). Ages within Glacier Bay, at greater distance from the fault, are more variable. Although cooling ages are typically young (2-5 Ma) and suggest Pliocene cooling for much of the area, several samples from the Lamplugh pluton (MGB3-6) are older and

complicate interpretation of cooling patterns. Three samples are along a small vertical transect (MGB4-6, ~250 m relief), but age reproducibility for two of these is poor and the lowest sample actually has the oldest age (Figure 19). The other sample from this area is much older and requires special interpretation (see below). Ignoring these four Lamplugh samples, it appears that ages increase to the south within Glacier Bay (Figure 20). Further analysis of this rough pattern would require additional sampling.

Several of the samples reproduced more poorly than the ±10% (2σ) analytical precision typically assumed for AHe ages (Table 1). This is common for AHe dating of extremely young samples, and can be due to low He concentrations, U and Th zoning, and overall poor separate quality. Of particular note are AHe replicates with standard deviations > 10% (1σ). Of the 10 samples north of the Alsek River, four have 1-σ reproducibilites between ±10% and ±15%. All other samples reproduce at better than 10%. Poor reproducibility of 03PH305A may be due both to low helium concentrations in several aliquots and to poor grain quality. Samples 03PH306A and 03PH307A had high quality grains with extremely high U and Th concentrations. Thus, the poor reproducibility is somewhat surprising and may be due to U and Th zoning. Sample 03PH311A was the youngest of the samples and the ±12.7% 1-σ uncertainty corresponds to only ±0.11 Ma age uncertainty. There are three problematic samples in Glacier Bay. MGB4 and MGB6 were both taken from the Lamplugh pluton along the east edge of the Border Ranges shear zone (BRSZ). This pluton is highly deformed and has been heavily chloritized (Roeske et al., 1990). Although the AHe thermochronometer seems to be largely independent of apatite composition (e.g. Farley et al., 2001), the effect of such extreme chloritization on AHe ages is not known. However, samples MGB3 and MGB5 were also taken from the Lamplugh pluton and reproduce well. Thus, poor separate quality (note high F_T for MGB6) may be the dominant factor causing poor sample reproducibility. MGB12 yielded small apatite crystals and the larger grains picked were generally of poor quality. Additionally, helium concentrations were low, thus poor reproducibility is expected.

The anomalously old age (17.9 Ma) of sample MGB3 is also difficult to explain in light of other ages in the Fairweather corridor. The sample is from the heavily deformed Lamplugh pluton, and sample alteration may have affected the AHe system

(Figure 21). However, the reproducibility of the sample (± 1.4%, 1-σ) suggests the age is robust. The old age is not likely a result of movement along the Border Ranges fault, as the fault has not been active since at least 33 Ma (Smart et al., 1996). Differential exhumation in the region could account for the old age. If a partial retention zone lies above most samples in Glacier Bay, then a pocket of slightly less recent exhumation could result in an old age. This hypothesis could further be tested with a vertical transect or by dating existing samples with higher closure temperature systems (e.g. AFT, ZHe). Extreme differential rock uplift along unrecognized structures seems an unlikely cause of the old age. The structural orientation needed to accommodate such uplift would suggest a structure running through the west arm of Glacier Bay, but other ages are young on both sides of the arm. Another possibility is that the sample was taken from a block recently displaced from a higher elevation. This was not indicated by field relations; however, the extreme relief and seismic activity in the area could have resulted in displacement of a large block. Because of a lack of a clear explanation for this anamolous age, we exclude it from further discussion.

Figure Captions:

Table 1: AHe ages for the Fairweather corridor. Seventeen-nine analyses and 22 samples ages are reported. Techniques and errors are discussed in the text and table footnotes.

Figure 13: Map of new AHe ages and the AFT ages previously measured in the Fairweather corridor by O'Sullivan et al. (1997). Background map is Figure 3.

Figure 14: AFT and AHe ages plotted against distance along the Fairweather fault, from Mt. Vancouver in the north to Cross Sound in the south. No cooling pattern is evident and young ages persist to the south end of the fault. Error bars are plotted as the 1-σ uncertainty based on replicate samples (Table 1).

Figure 15: AFT and AHe ages plotted against distance from the Fairweather fault. Old ages (> 5 Ma) are more common at greater distances from the fault, but ages < 3 Ma are found 50 km from the fault. AHe error bars are plotted as the 1-σ uncertainty based on replicate samples (Table 1).

Figure 16: Young AHe ages cluster around the northern terminus of the Fairweather fault where structures bend to the west. The zone of rapid cooling is poorly defined, but is inferred to widen to the west based on young ages in Icy Bay and a young age on Mt. St. Elias (Spotila et al., 2004; O'Sullivan et al., 1997). Locations of faults are from Bruhn et al. (2004); FF-Fairweather fault; BF-Boundary fault; BRFS-Border Ranges fault system; ECF-Esker Creek fault; CSEF-Chugach-St. Elias fault. Area location shown in Figure 13.

Figure 17: Age versus elevation plot of the samples adjacent to and north of the Alsek River. O'Sullivan noted an increase in age with elevation, however, the pattern was diffuse and the trend line is not plotted. AHe ages show no age-elevation pattern with the youngest age at 1610 m.

Figure 18: Plot of AFT-AHe age pairs of samples obtained from O'Sullivan. A closure temperature (T_c) of 110º C is inferred for all AFT analysis (O'Sullivan et al., 1997) and the T_c for AHe ages varies based on cooling rate and grain size (Table 1).

Figure 19: Age versus elevation plot of samples on Mt. Parker in Glacier Bay. Samples have large error bars and no reliable exhumation rate can be inferred from the data.

Figure 20: AHe ages plotted against north-south distance in Glacier Bay. Sample ages increase linearly from 2.31 Ma in Johns Hopkins Inlet to 5.69 Ma in Cross Sound.

Figure 21: Map of Lamplugh pluton with AHe samples plotted. Ar/Ar age and mapping are from Roeske et al. (1992) and Smart et al. (1996). Background map is from the 3 arc second Shuttle Radar Topography Mission data available at http://seamless.usgs.gov. Area location is shown in Figure 13.

Table 1

Sample	Elevation m	Latitude	Longitude	K/Ar, Ar/Ar, U/Pb age (Ma)	Rock Type	mass mg	MWAR _m	He4 pmol	U ppm	Th ppm	# of Grains	FT	Tc °C	Age Ma	Avg. Age Ma	±1_ %
03PH305A-1	88	59.1281	138.0839	48.2±6 (b) †*	Tonalite	0.0055	69.0	0.0006	7.2	10.2	1	0.82	76	2.65 _		
03PH305A-2						0.0030	46.0	0.0004	22.1	11.5	1	0.75	75	1.35 _		
03PH305A-3						0.0047	54.0	0.0006	14.5	10.4	2	0.77	75	1.72 _	**1.93**	**24.06**
03PH305A-4						0.0104	48.3	0.0010	11.7	11.1	5	0.74	75	1.66 _		
03PH305A-7						0.0339	50.7	0.0152	42.3	30.4	15	0.77	70	2.25		
03PH306A-1	67	59.4272	138.1097	32.0±1.9 (b) ‡*	Tonalite	0.0105	48.6	0.0016	6.3	6.8	5	0.78	66	4.72 _		
03PH306A-2				34.7±1.0 (z) †*		0.0103	53.4	0.0024	12.4	5.2	4	0.76	68	4.24 _	**5.11**	**12.80**
03PH306A-3						0.0112	44.9	0.0022	7.2	8.2	5	0.73	64	5.67 _		
03PH306A-4						0.0146	48.0	0.0023	5.8	6.0	7	0.73	64	5.81		
03PH307A-1	243	59.4378	138.2492	Tertiary?	Granodiorite	0.0210	51.3	0.0288	125.9	199.2	7	0.75	73	2.01	**2.34**	**13.92**
03PH307A-3						0.0189	44.0	0.0466	182.7	273.2	9	0.72	69	2.66		
03PH309A-1	741	59.4044	138.6967	Tertiary?	Orthogneiss	0.0098	41.6	0.0018	15.5	18.7	7	0.72	69	2.39 _		
03PH309A-2						0.0056	38.8	0.0009	14.4	10.2	5	0.71	67	2.72 _	**2.56**	**6.46**
03PH309A-3						0.0039	50.6	0.0012	6.6	18.9	1	0.77	64	7.05 _		
03PH309A-4						0.0053	34.7	0.0024	11.1	4.6	5	0.68	55	10.5		
03PH310A-1	926	59.9417	139.2331	51.1±3 (hb) †*	Granodiorite	0.0031	30.3	0.0015	71.0	130.9	5	0.60	67	1.55 _		
03PH310A-2						0.0102	37.8	0.0057	69.3	104.2	11	0.69	70	1.64	**1.67**	**6.97**
03PH310A-3						0.0053	38.2	0.0035	69.7	134.1	5	0.68	70	1.83 _		
03PH311A-1	1610	60.0225	139.2058	Tertiary?	Granite	0.0134	45.0	0.0011	27.4	3.1	8	0.74	79	0.73		
03PH311A-2						0.0191	52.5	0.0022	28.8	5.6	8	0.77	79	0.97	**0.89**	**12.71**
03PH311A-3						0.0120	46.7	0.0016	33.5	4.1	6	0.74	78	0.97		
80APR49A-1	2150	59.8967	138.9033	36.2±1.4 (b) †	Tonalite	0.0130	44.1	0.0013	19.8	8.4	8	0.74	75	1.22		
80APR49A-2				37.1±1.4 (b) †		0.0120	40.5	0.0019	35.2	9.5	10	0.70	74	1.14	**1.13**	**6.89**
80APR49A-3						0.0168	44.4	0.0030	45.2	7.1	11	0.72	76	1.03		
69APR32A-1	2499	60.3017	139.6017	46.8±1 (m) †	Granodiorite	0.0123	63.9	0.0023	23.2	8.5	3	0.80	72	1.75	**1.90**	**7.65**
69APR32A-2				44.6±1 (b) †		0.0099	43.0	0.0009	12.1	2.2	7	0.72	71	2.04 _		

Table 1 continued.

Sample	Elevation	Latitude	Longitude	K/Ar, Ar/Ar, U/Pb age (Ma)	Rock Type	mass	MWAR	He4	U	Th	# of Grains	FT	Tc	Age	Avg. Age	±1_
	m					mg	_m	pmol	ppm	ppm			°C	Ma	Ma	%
69APR31B-1	1829	60.2867	139.1983	279±8 (hb) †	Diorite	0.0260	117.3	0.0053	6.9	15.8	1	0.91	66	3.99		
69APR31B-2						0.0174	98.9	0.0025	4.8	14.0	1	0.89	66	3.79		
69APR31B-3						0.0157	72.0	0.0044	10.5	23.7	2	0.85	66	3.88	**3.62**	**9.31**
69APR31B-4						0.0100	43.2	0.0025	13.6	28.2	7	0.75	68	3.16		
69APR31B-5						0.0143	44.5	0.0054	19.3	41.6	9	0.75	67	3.27		
MGB1-1	0	58.7573	136.2563	Cretaceous	Granite	0.0234	44.2	0.0059	13.4	16.9	14	0.73	66	3.76		
MGB1-2						0.0159	48.8	0.0040	11.6	15.4	8	0.75	67	4.16	**3.84**	**6.04**
MGB1-3						0.0148	38.5	0.0061	14.9	19.9	13	0.69	61	5.81		
MGB1-4						0.0201	49.7	0.0047	12.6	17.3	8	0.74	68	3.61		
MGB2-1	0	58.8959	136.6648	Cretaceous	Granite	0.0202	42.8	0.0118	64.7	42.6	12	0.71	70	2.11		
MGB2-2						0.0224	69.7	0.0194	63.7	42.5	3	0.82	76	2.74		
MGB2-3						0.0192	58.3	0.0106	50.8	36.4	4	0.79	74	2.25	**2.50**	**12.04**
MGB2-4						0.0462	59.8	0.0341	67.0	43.3	10	0.78	74	2.36		
MGB2-5						0.0462	63.4	0.0402	70.5	48.1	8	0.80	75	2.56		
MGB2-6						0.0596	98.7	0.0451	48.4	30.8	4	0.87	80	3.00		
MGB3-1	0	58.9718	136.9458	123.3±0.4 (hb) †*		0.0114	42.4	0.0178	16.9	28.8	7	0.70	55	17.9		
MGB3-2						0.0160	67.9	0.0198	11.6	19.6	3	0.81	61	18.2	**17.9**	**1.28**
MGB3-3						0.0155	63.3	0.0206	13.0	21.1	3	0.80	60	17.6		
MGB4-1	232	58.8899	136.9171	123.3±0.4 (hb) †*		0.0126	59.4	0.0132	23.0	37.7	3	0.79	65	7.83		
MGB4-2						0.0115	46.6	0.0109	32.4	42.2	6	0.75	64	5.70	**6.06**	**19.93**
MGB4-3						0.0167	48.7	0.0101	16.2	28.4	9	0.74	63	6.85		
MGB4-4						0.0123	43.8	0.0102	26.1	46.5	8	0.75	63	5.69		
MGB4-5						0.0246	50.2	0.015	27.3	39.6	11	0.75	67	4.25		
MGB5-1	128	58.8941	136.9230	123.3±0.4 (hb) †*		0.0194	44.3	0.0114	18.6	34.9	13	0.71	63	5.91		
MGB5-2						0.0170	43.9	0.0140	27.1	45.7	11	0.73	63	5.67	**5.90**	**7.05**
MGB5-3						0.0182	44.9	0.0121	21.1	43.6	10	0.74	64	5.45		
MGB5-4						0.0147	54.1	0.0152	27.0	49.0	4	0.78	65	6.56		
MGB6-1	0	58.8982	136.9256	123.3±0.4 (hb) †*		0.0079	28.9	0.0070	25.7	30.2	15	0.58	54	8.97		
MGB6-2						0.0120	39.3	0.0110	18.5	29.0	10	0.70	58	9.79	**8.14**	**17.69**
MGB6-3						0.0140	65.0	0.0127	30.7	26.3	3	0.79	69	5.95		
MGB6-4						0.0182	48.1	0.0196	28.2	27.8	10	0.75	62	7.85		

Table 1 continued.

Sample	Elevation	Latitude	Longitude	K/Ar, Ar/Ar, U/Pb age (Ma)	Rock Type	mass	MWAR	He4	U	Th	# of Grains	FT	Tc	Age	Avg. Age	±1_
	m					mg	_m	pmol	ppm	ppm			°C	Ma	Ma	%
MGB7-1	0	58.8484	137.1213	Tertiary or		0.0161	59.3	0.0044	26.8	17.9	7	0.79	75	2.15	**2.31**	**6.93**
MGB7-2				Cretaceous		0.0142	51.7	0.0027	16.5	9.8	7	0.77	72	2.47		
MGB8-1	0	58.7254	136.4105	Cretaceous		0.0130	43.5	0.0091	69.2	53.3	8	0.71	70	2.32	**2.15**	**8.16**
MGB8-2						0.0180	42.8	0.0116	74.5	56.4	11	0.71	71	1.97		
MGB9-1	0	58.6066	136.4647	Cretaceous	Granite	0.0153	41.7	0.0094	36.6	28.7	9	0.70	65	3.84		
MGB9-2						0.0285	45.5	0.0157	37.1	33.4	15	0.72	68	3.25		
MGB9-3						0.0250	45.2	0.0165	29.6	26.2	13	0.72	65	4.89	**4.20**	**18.21**
MGB9-4						0.0252	46.4	0.0152	34.1	33.3	14	0.73	67	3.74		
MGB9-5						0.0316	49.1	0.0236	29.6	24.8	14	0.76	65	5.30		
MGB10-1	0	58.3315	136.2065	Cretaceous		0.0287	71.0	0.0115	11.8	17.8	3	0.81	70	5.88		
MGB10-2						0.0302	80.2	0.0179	8.5	15.4	2	0.84	67	11.1	**5.69**	**2.66**
MGB10-3						0.0222	49.3	0.0093	14.7	20.6	8	0.74	65	5.51		
MGB10-4						0.0265	54.6	0.0095	11.5	17.3	6	0.77	66	5.67		
MGB11-1	0	58.2800	136.7756	Tertiary		0.0070	43.8	0.0028	37.7	16.4	4	0.71	69	2.52 _	**2.83**	**10.80**
MGB11-2						0.0123	65.6	0.0032	12.4	28.2	2	0.83	74	3.13 _		
MGB12-1	0	58.3979	137.0723	Mid Tertiary	Sandstone	0.0115	41.9	0.0014	15.6	22.2	8	0.70	72	1.61 _		
MGB12-2						0.0110	41.4	0.0007	20.0	17.6	9	0.70	77	0.77 _		
MGB12-3						0.0161	42.8	0.0016	49.1	32.3	13	0.70	64	4.66 _	**0.93**	**54.63**
MGB12-4						0.0171	47.4	0.0005	21.4	32.6	10	0.74	70	2.54 _		
MGB12-5						0.0115	40.3	0.0019	90.7	100.8	10	0.69	82	0.40 _		
95APo21-1	0	59.8144	138.9167	54±? (z) §	Granite	0.0105	39.9	0.0019	22.2	8.1	9	0.71	69	2.05 _	**2.15**	**4.43**
95APo21-2						0.0149	43.5	0.0039	29.4	5.2	10	0.73	70	2.24		

All sample uncertainties are reported as the standard deviation (1_) based on replicates.

Underlined aliquot ages are anomalous for the given sample based on replicates and are not included in the average age calculation.

_ AHe age with uncertainty He blank correction > 10% of total He gas (2_).

† K/Ar age compiled by Wilson et al. (1994) Dated mineral phases shown in parentheses: b-biotite, m-muscovite, hb-hornblende, z-zircon

‡ K/Ar age from Campbell and Dodds (1988); § U/Pb age from Sisson et al. (2003); # Ar/Ar age from Roeske et al. (1990)

* represents age taken from within the same pluton but not on the same rock sample

Samples from plutons without high temperature age constraints are listed with inferred age from petrography and field relations (Brew and Morrell, 1983; Plafker et al., 1994)

MGB samples collected by McAleer (2005); 03PH samples collected by Peter Hauessler (2003); 95APo from Terry Pavlis; APR samples from Paul O'Sullivan

Figure 13

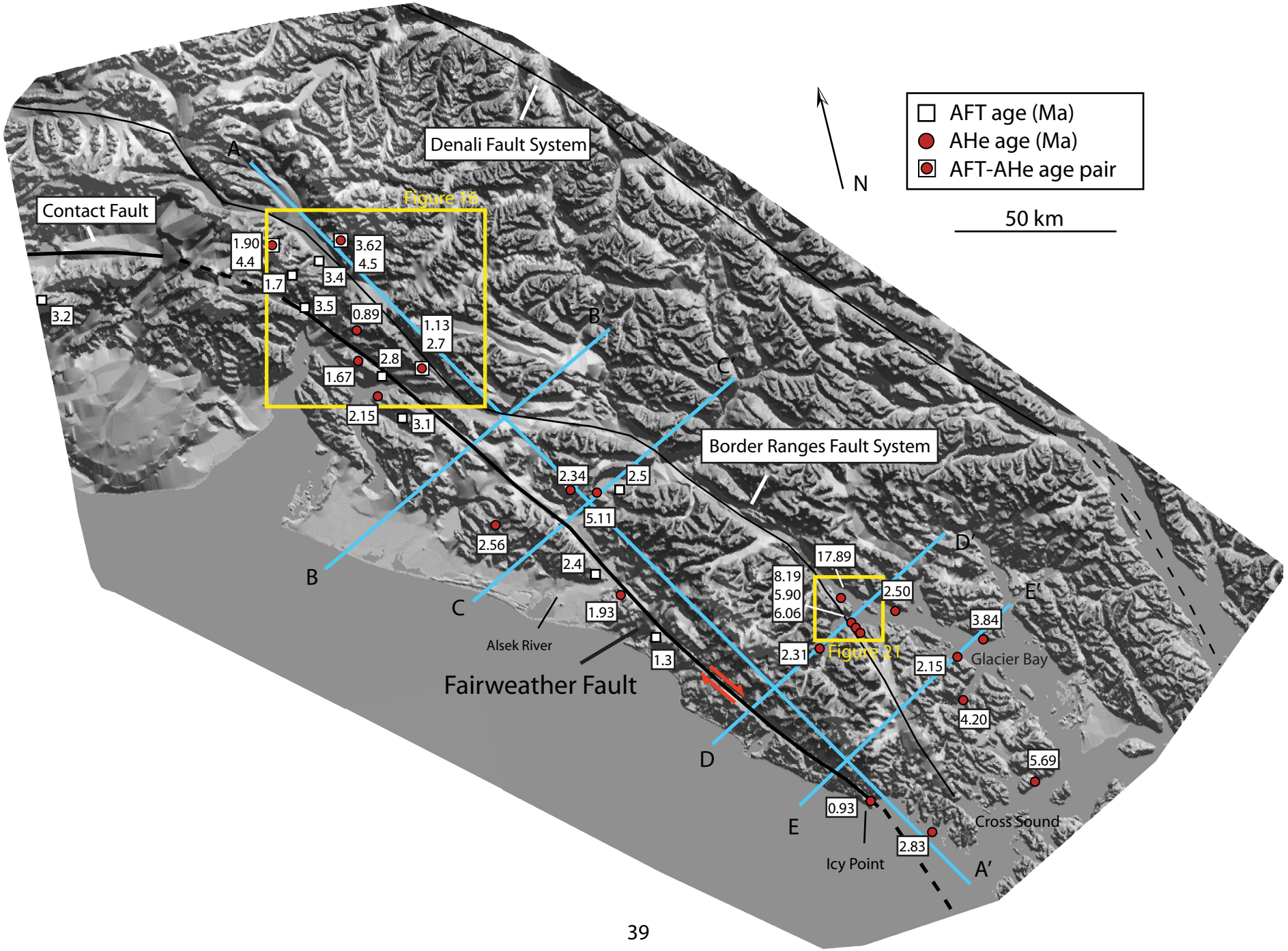
Denali Fault System
Contact Fault
Figure 16
Border Ranges Fault System
Fairweather Fault
Alsek River
Figure 21
Glacier Bay
Cross Sound
Icy Point
A
A′
B
B′
C
C′
D
D′
E
E′
N
AFT age (Ma)
AHe age (Ma)
AFT-AHe age pair
50 km
1.90
4.4
3.62
4.5
1.7
3.4
3.2
3.5
0.89
1.13
2.7
2.8
1.67
2.15
3.1
2.34
2.5
5.11
2.56
2.4
1.93
1.3
17.89
8.19
5.90
6.06
2.50
2.31
3.84
2.15
4.20
5.69
0.93
2.83

Figure 14

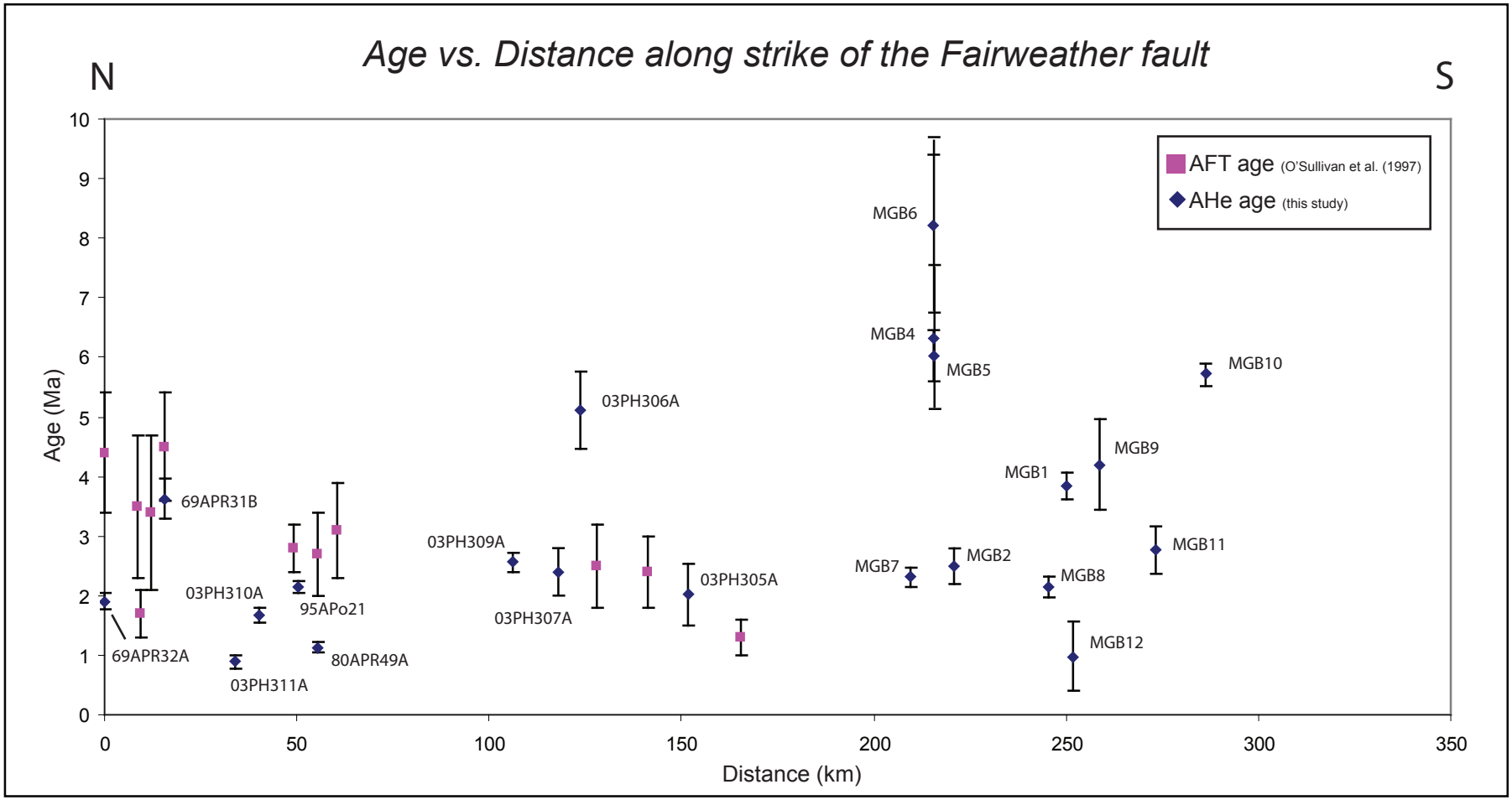
Age vs. Distance along strike of the Fairweather fault
N
S
AFT age (O'Sullivan et al. (1997)
AHe age (this study)
Age (Ma)
Distance (km)
0
1
2
3
4
5
6
7
8
9
10
0
50
100
150
200
250
300
350
MGB6
MGB4
MGB5
MGB10
MGB9
MGB1
MGB11
MGB7
MGB2
MGB8
MGB12
03PH306A
03PH309A
03PH307A
03PH305A
03PH310A
95APo21
69APR31B
69APR32A
80APR49A
03PH311A

Figure 15

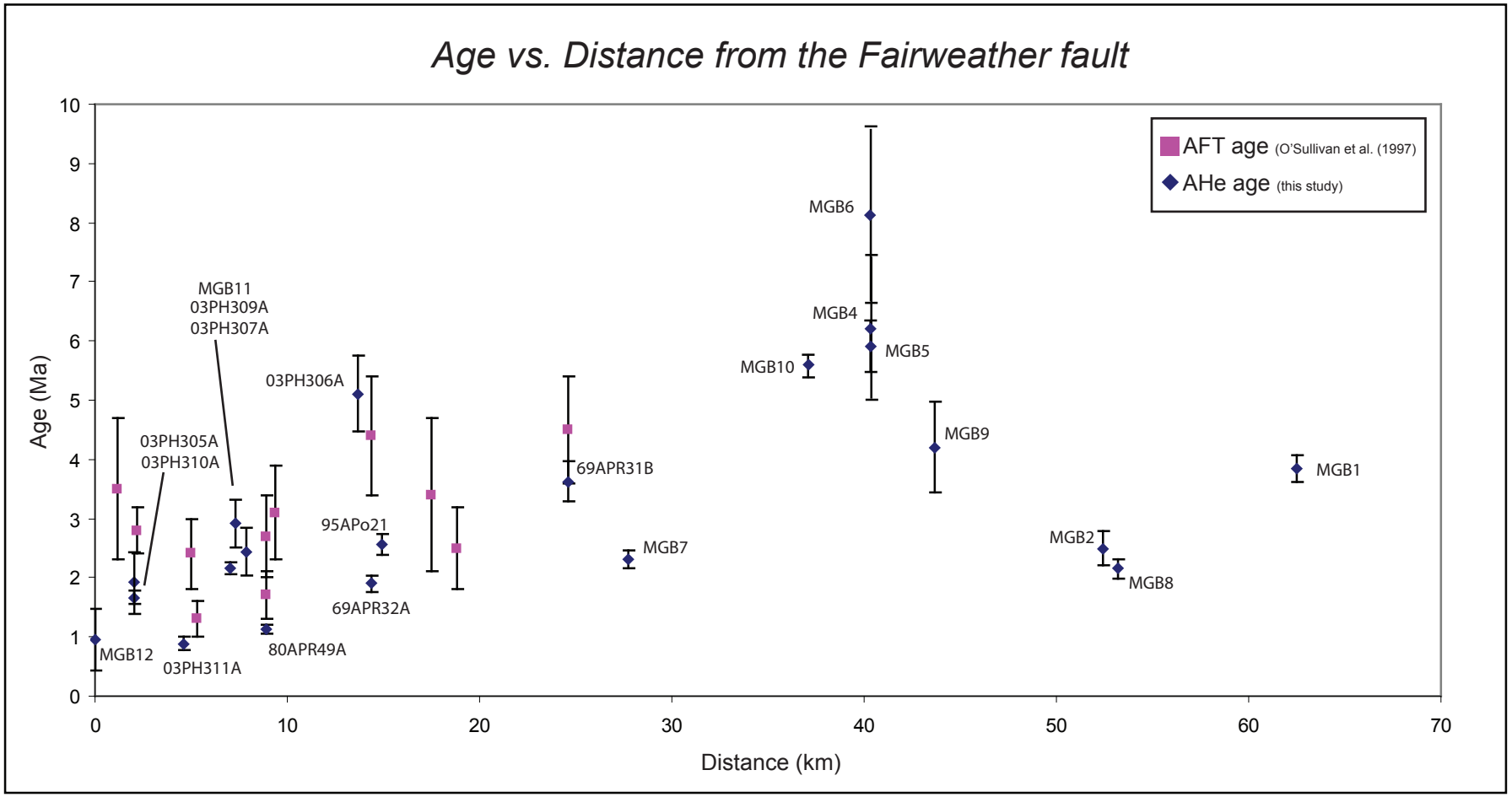
Age vs. Distance from the Fairweather fault
AFT age (O'Sullivan et al. (1997)
AHe age (this study)
Age (Ma)
Distance (km)
0
1
2
3
4
5
6
7
8
9
10
0
10
20
30
40
50
60
70
MGB12
03PH311A
MGB11
03PH309A
03PH307A
03PH305A
03PH310A
80APR49A
03PH306A
95APo21
69APR32A
69APR31B
MGB7
MGB6
MGB4
MGB5
MGB10
MGB9
MGB2
MGB8
MGB1

Figure 16

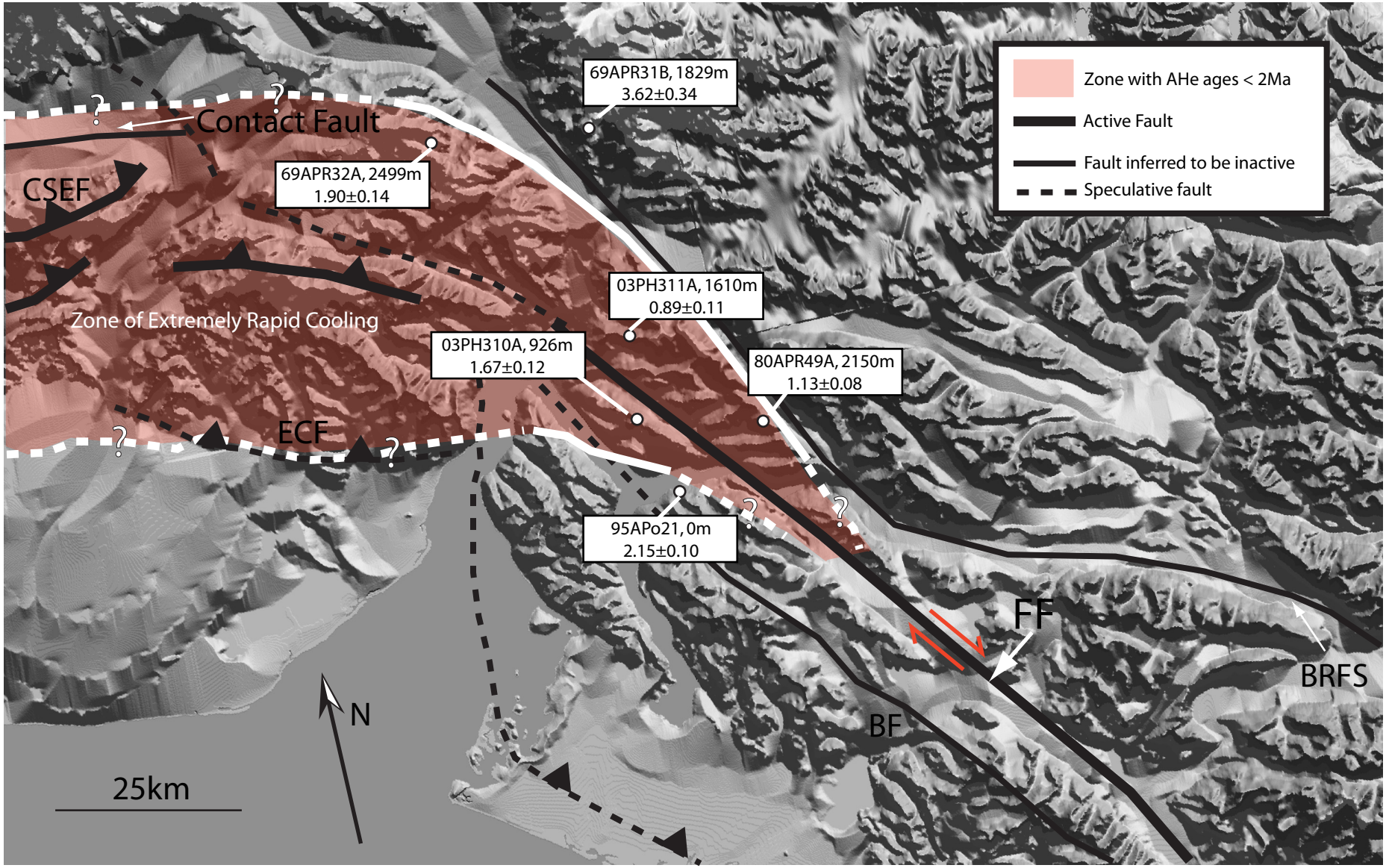
Contact Fault
CSEF
69APR32A, 2499m
1.90±0.14
69APR31B, 1829m
3.62±0.34
03PH311A, 1610m
0.89±0.11
03PH310A, 926m
1.67±0.12
80APR49A, 2150m
1.13±0.08
Zone of Extremely Rapid Cooling
ECF
95APo21, 0m
2.15±0.10
FF
BRFS
BF
N
25km
Zone with AHe ages < 2Ma
Active Fault
Fault inferred to be inactive
Speculative fault

Figure 17

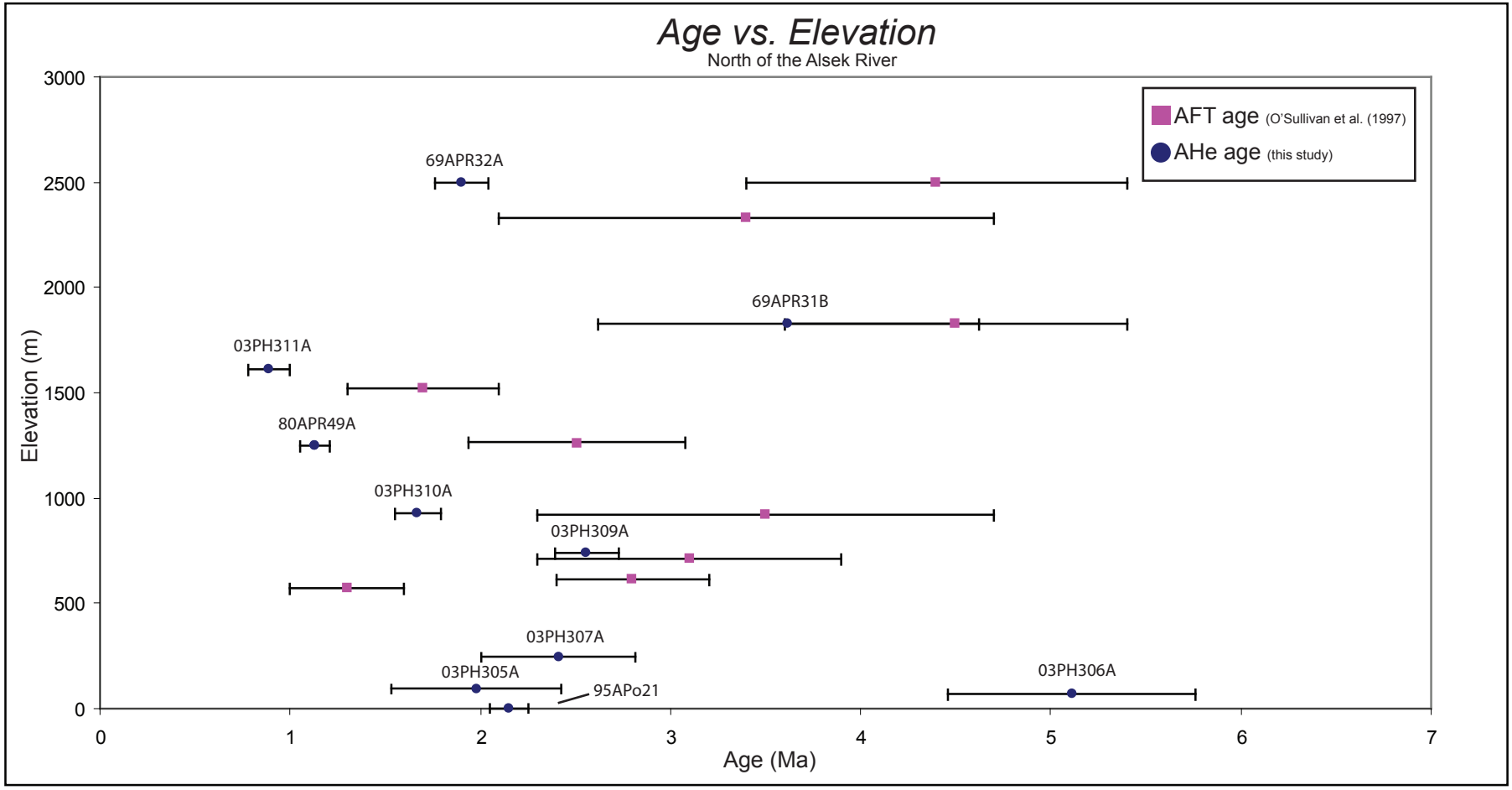
Age vs. Elevation
North of the Alsek River
AFT age (O'Sullivan et al. (1997)
AHe age (this study)
69APR32A
69APR31B
03PH311A
80APR49A
03PH310A
03PH309A
03PH307A
03PH305A
95APo21
03PH306A
Elevation (m)
Age (Ma)
0
500
1000
1500
2000
2500
3000
0
1
2
3
4
5
6
7

Figure 18

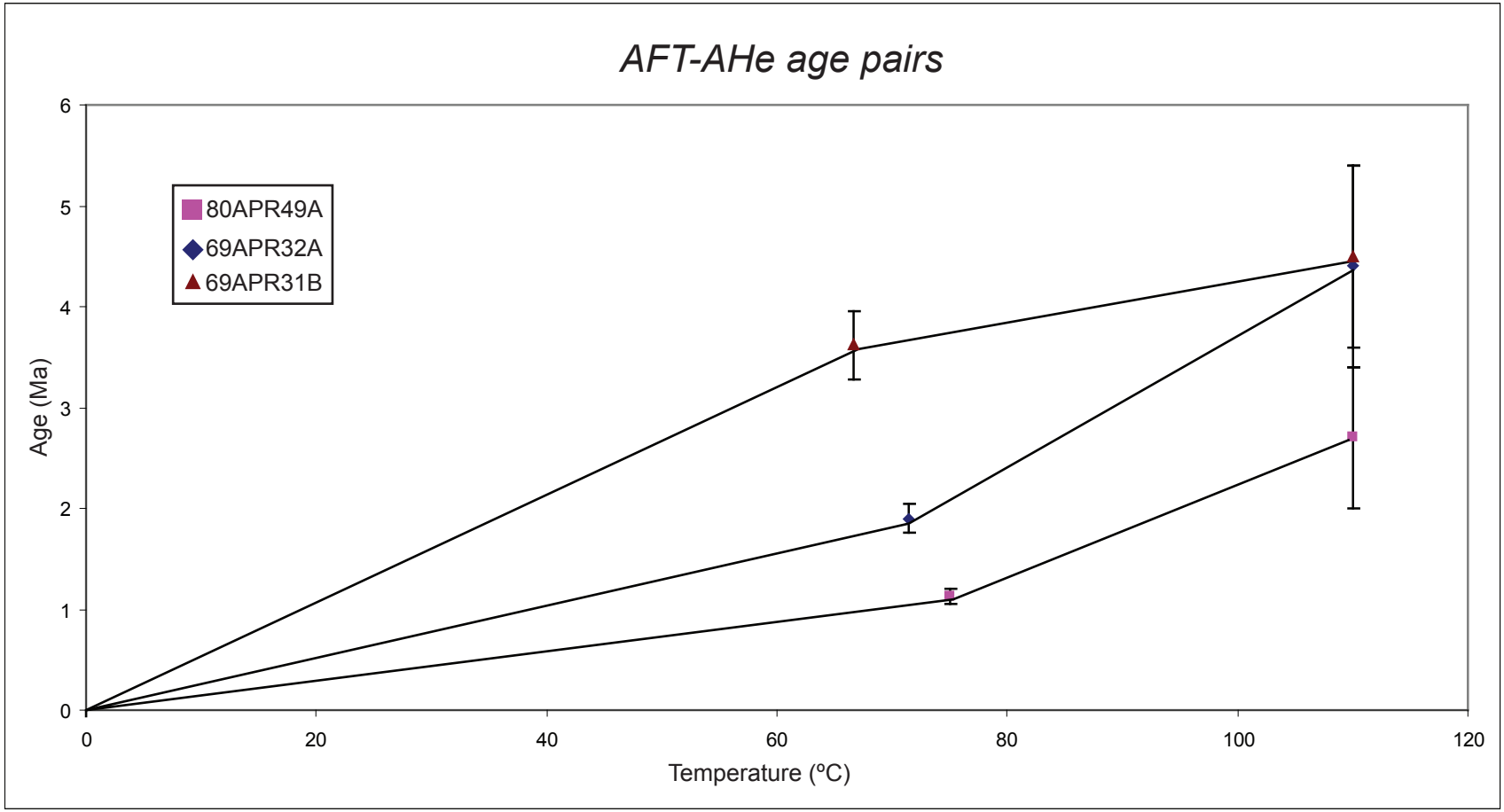
AFT-AHe age pairs
80APR49A
69APR32A
69APR31B
Age (Ma)
Temperature (ºC)
0
1
2
3
4
5
6
0
20
40
60
80
100
120

Figure 19

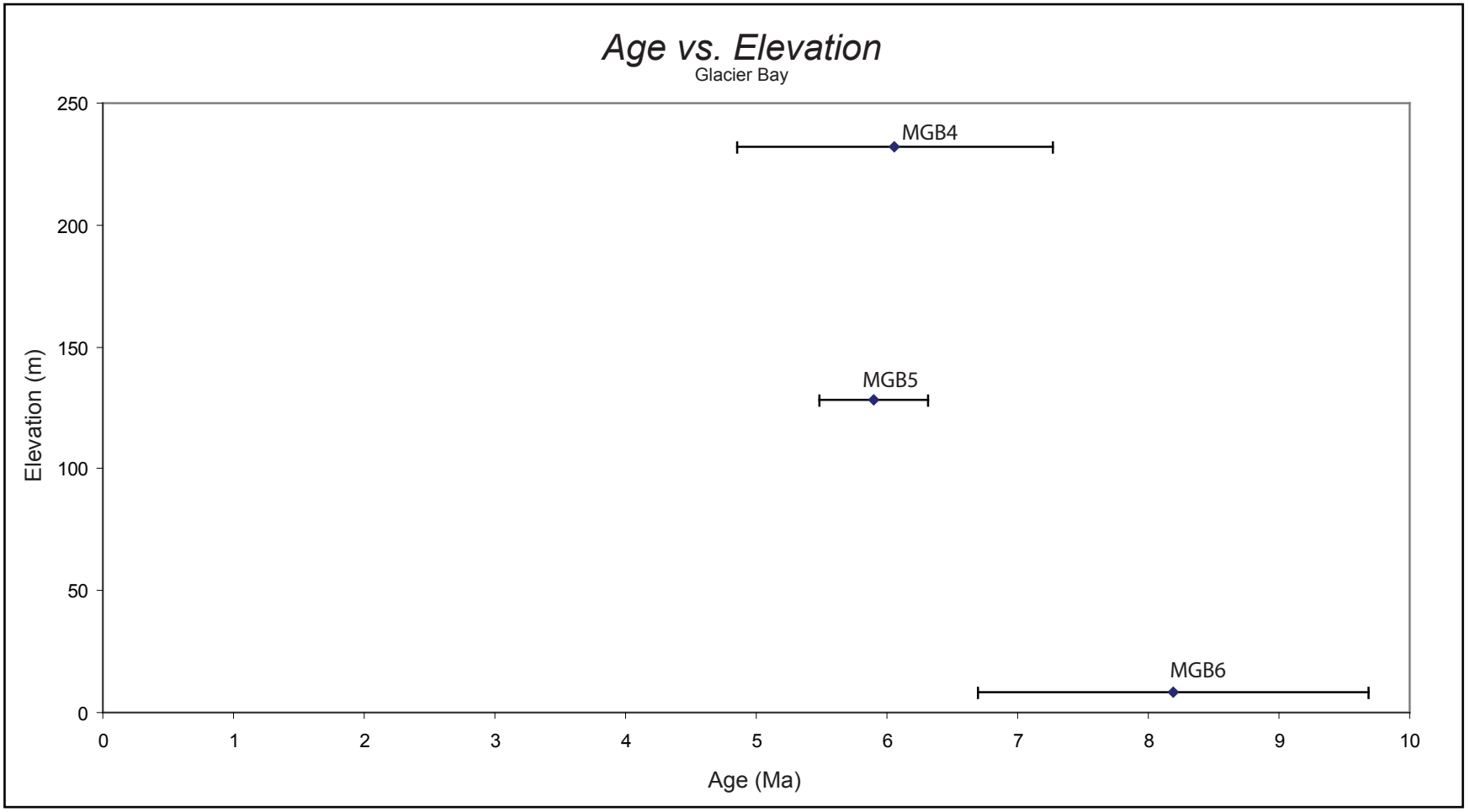
Age vs. Elevation
Glacier Bay
250
200
150
100
50
0
Elevation (m)
MGB4
MGB5
MGB6
0
1
2
3
4
5
6
7
8
9
10
Age (Ma)

Figure 20

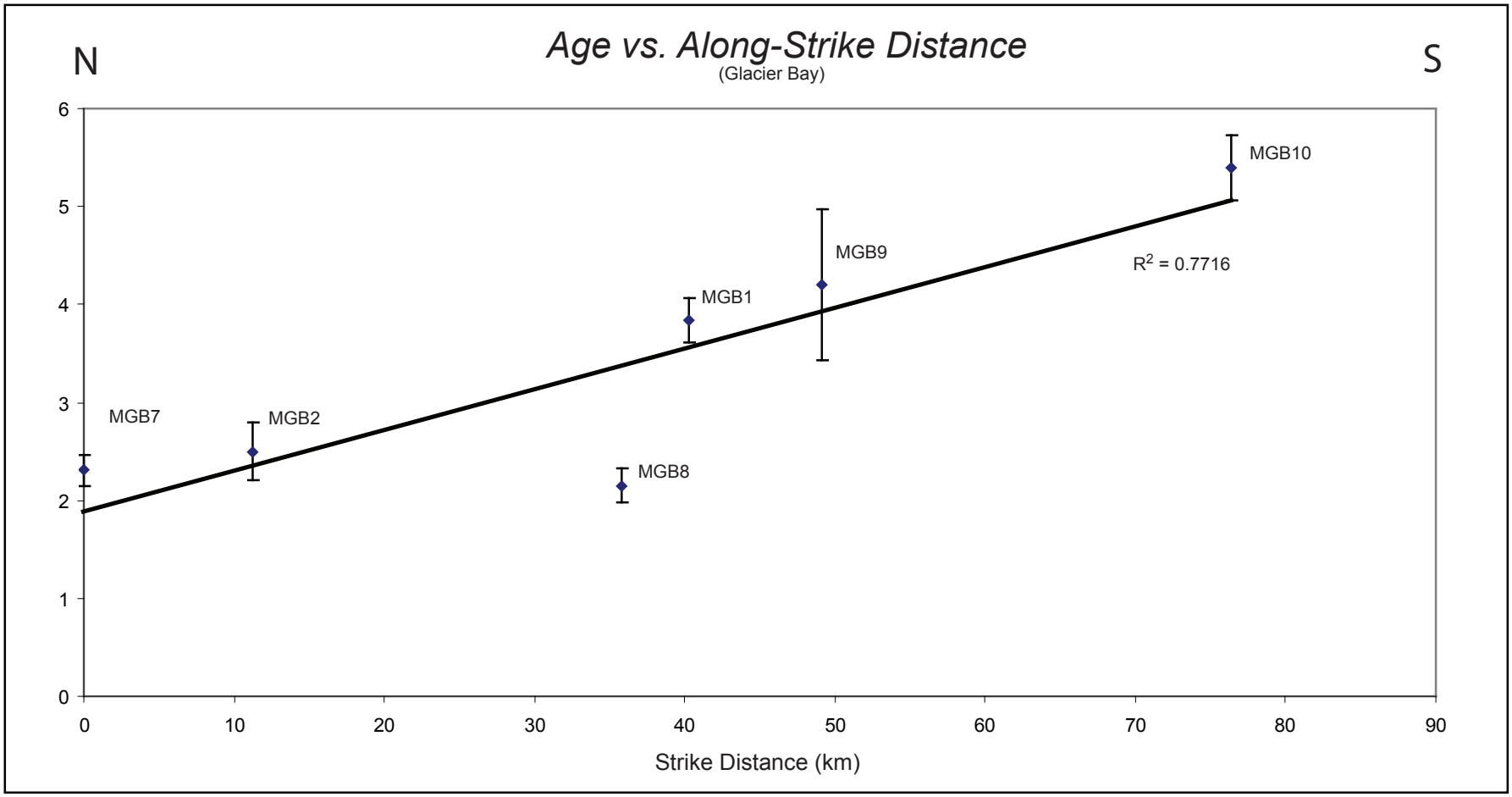
N
Age vs. Along-Strike Distance
(Glacier Bay)
S
MGB10
MGB9
MGB1
MGB7
MGB2
MGB8
R2 = 0.7716
0
1
2
3
4
5
6
0
10
20
30
40
50
60
70
80
90
Strike Distance (km)

Figure 21

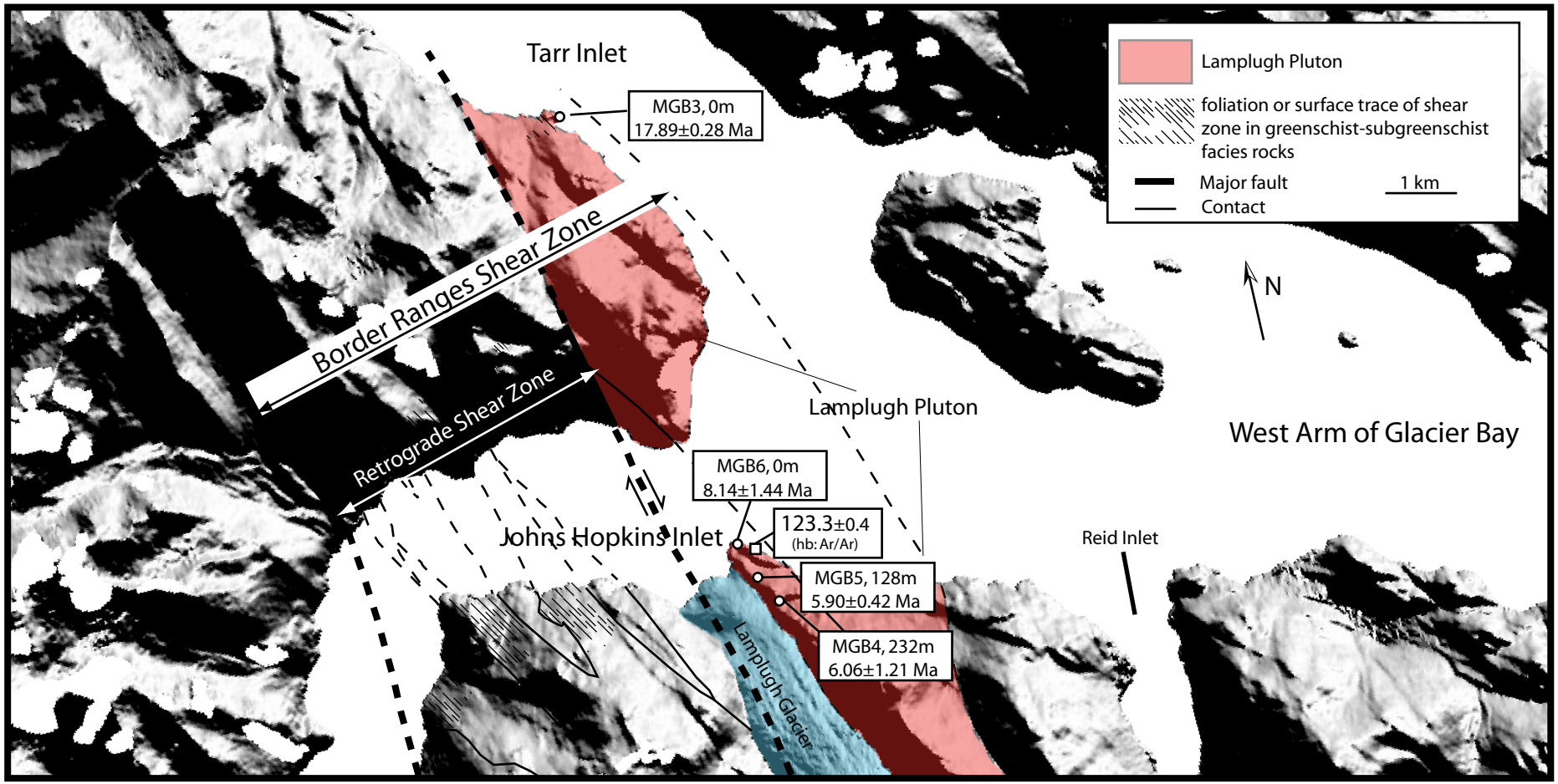
Tarr Inlet
MGB3, 0m
17.89±0.28 Ma
Border Ranges Shear Zone
Retrograde Shear Zone
Lamplugh Pluton
West Arm of Glacier Bay
MGB6, 0m
8.14±1.44 Ma
123.3±0.4
(hb: Ar/Ar)
Johns Hopkins Inlet
Reid Inlet
MGB5, 128m
5.90±0.42 Ma
MGB4, 232m
6.06±1.21 Ma
Lamplugh Glacier
N
Lamplugh Pluton
foliation or surface trace of shear zone in greenschist-subgreenschist facies rocks
Major fault
Contact
1 km

5. Discussion

AHe ages reveal a zone of rapid cooling in the Fairweather corridor. New ages in previously unsampled Glacier Bay indicate this zone is > 50 km wide and extends the onshore length of the Fairweather fault. The resolved cooling rates and patterns have implications for the role of the Fairweather corridor and the Transition fault in YT accretion, place constraints on the timing and driving forces behind rapid cooling, and put modern uplift and erosion rates into a geologic context.

5.1 Inferring Exhumation

Inferring exhumation from thermochronologic data requires knowledge of the geothermal gradient through time. Unfortunately, onshore surface heat flow measurements do not exist within the Fairweather corridor. Thus, the current geothermal gradient must be estimated from thermal data in offshore wells, which record a maximum gradient of 25ºC/km (Flett, 1992; Johnsson et al., 1992). The geothermal gradient in the Late Miocene and Pliocene, prior to the cooling of most of the Fairweather samples, is estimated at 36ºC/km from an exhumed AFT partial annealing zone on Mt. Logan, ~100 km northwest of the field area (O'Sullivan and Currie, 1996). Additionally, O'Sullivan et al. (1997) estimate a Late Cenozoic, time-averaged, gradient of 25ºC/km based on the age-elevation relationship between AFT samples spaced throughout the northern Fairweather corridor. Here we assume a slightly higher time-averaged gradient of 30ºC/km, and make the simplifying assumption of a topography-parallel closure isotherm. This assumption may lead to an overestimation of exhumation rates in valleys and an underestimate in ridges (Stuwe et al., 1994). However, the lack of local thermal constraints and the unknown effect of fluid flow on the thermal field (Ehlers, 2005) preclude an analysis of the geothermal gradient on a sample to sample basis. A 30ºC/km gradient corresponds to a closure depth of 2.2-2.5 km for the estimated closure temperature of most samples. At these closure depths, sample ages correspond to localized exhumation rates as high as 3 mm/yr, with average rates closer to 1 mm/yr (Figure 22). These exhumation rates are much faster than rates at passive margins (<< 0.1 mm/yr; e.g. Spotila et al., 2004), but are slower than rates in New Zealand and Nanga

Parbat (e.g. Little et al., 2005; Schneider et al., 1999) and are not sufficient to suggest significant perturbation of the thermal field due to heat advection (Mancktelow and Grasemann, 1997).

5.2 Regional Implications

Exhumation rates on the order of ~1 mm/yr surround nearly the entire onshore length of the Fairweather fault, including the southernmost onshore portion, 280 km from the core of the St. Elias orogen. This suggests that motion of the YT has been oblique to the Fairweather corridor over the past few million years resulting in transpressional tectonics, and that slip is partitioned between strike-slip motion on the Fairweather fault and pure shear deformation on yet unrecognized structures. Existing samples elucidate no regional pattern in exhumation relative to mapped faults. Rates are rapid at great distances from (> 50 km), and in close proximity to (< 5km), the Fairweather fault, and exhibit no consistent change across terrane boundaries. Exhumation rates may decrease slightly away from the Fairweather fault, but this pattern is not consistent (Figure 14). Local variations from the regional exhumation rate occur near Yakutat Bay and Glacier Bay. North of Yakutat Bay, near the termination of the Fairweather fault, the youngest AHe ages correspond to a bend in active structures from northwest trending strike-slip faults to east-west trending thrusts, resulting in contraction and uplift as evidenced by the observed increase in topographic relief (Pavlis et al., 2004). The maximum exhumation rates of 2-3 mm/yr near Yakutat Bay are likely caused by motion into this bend towards the St. Elias orogen. Exhumation rates in Glacier Bay appear to decrease from ~1 mm/yr in Johns Hopkins Inlet to 0.4 mm/yr in Cross Sound (Figure 19). This could result from decreasing convergence due to the more northerly (PA-NA parallel) orientation of the Fairweather fault south of Icy Point (Figure 2), and/or increased activity at the southeast end of the Transition fault (see below). Additional evaluation of regional and local patterns would require increased sample coverage and further delineation of active structures in the Fairweather corridor.

The estimated regional exhumation rate of ~1 mm/yr places a rough constraint on the magnitude of convergent plate motion accommodated in the Fairweather corridor. Although the extent of rapid exhumation is not well defined, young ages in Glacier Bay

(~50 km east of the Fairweather fault) and a young age in the Yakutat foothills (15 km west of the Fairweather fault) indicate that the zone of rapid exhumation is broad. Assuming a 65-km-wide zone of spatially-averaged ~1 mm/yr exhumation, a crustal thickness of the obliquely colliding YT of 15 km (Plafker et al., 1994), and flux steady state based on the ruggedness of topography (Willet and Brandon, 2002), ~4.3 mm/yr of convergence has been accommodated in the Fairweather corridor over the past few Ma (Figure 23a, b). This rate is less than the 16.8 mm/yr Fairweather fault-normal motion expected from the PA-NA vector (DeMets and Dixon, 1999), and implies that additional convergence must be accommodated elsewhere. However, there are numerous uncertainties in this rate comparison. Exhumation rates could easily be off by a factor of 2 due to geothermal consideration. The thickness of the colliding plate and width of the exhumation zone are also loosely constrained. It is also possible that the region is not in topographic steady-state, such that net crustal thickening has occurred over the past few Ma. However, continuous glaciation of the margin for much of the past 5 Ma and low mean elevation (< 1 km) (Figure 6, 7) throughout much of the Fairweather corridor indicate such crustal thickening has not accommodated that much convergence. Thus, although this estimate of convergence rate is only loosely constrained, it is likely that shortening and related exhumation in the Fairweather corridor accounts for only a small fraction of the Fairweather-normal component of PA-NA motion at million-year time scales.

This result is roughly consistent with GPS data. The ~4.3 mm/yr convergence rate combined with the geologic slip rate of 48 mm/yr on the Fairweather fault (Plafker et al., 1978), implies the vector of motion accommodation in the Fairweather corridor is 48.2 mm/yr, at N28.9°W, ~5° oblique to the Fairweather fault (Figure 23c). This is similar to the slip rate on the Fairweather fault and obliquity in the plate vector based on GPS (Fletcher and Freymueller, 2003). The rate of shortening is also consistent with a GPS derived model of shortening in which the effects of glacial rebound and strike-slip motion on the Fairweather fault have been removed (Larsen; personal comm., 2006). If these independent data sets are correct, YT motion is slightly oblique to the Fairweather corridor and rotated ~14° from the PA-NA vector (DeMets and Dixon, 1999). This implies motion on the YT-PA interface—the Transition fault.

If the Fairweather corridor accommodates only on the order of ~4 mm/yr Fairweather fault-normal motion via crustal shortening and exhumation, then it is likely that the missing convergence is accommodated outboard of the coastal region. The most obvious structure for accommodation of the remaining ~12 mm/yr convergence is the Transition fault, which is oriented at a high angle (64°) to the Fairweather fault. An oblique slip rate of 12 mm/yr could accommodate this convergence, which is compatible with 10 mm/yr late Cenozoic slip rates on the southeast part of the fault predicted by the microplate model of Pavlis et al. (2004). Current activity on the Transition fault is also supported by a series of earthquakes as large as M6.7, in 1973, which indicated thrusting of the Pacific plate beneath the YT at the Transition fault (Figure 2). However, the estimated slip rate from these earthquakes is only 3 mm/yr (Doser and Lomas, 2000). Such a high slip rate is also incompatible with numerical models of the Alaska deformation field (Lundgren et al., 1995; Bird, 1996). Furthermore, portions of the Transition fault are overlain by 800-m-thick Quaternary sediments, which indicate current fault inactivity (Pavlis et al., 2004). It is possible that slip rate has varied on the Transition fault, such that the rate averaged over the past few Ma has been rapid enough to accommodate the convergence unaccounted for by the Fairweather corridor. It is also possible that this shortening is accommodated elsewhere. Additional convergence may be accommodated by a strike-slip zone in the Pacific plate, where two M 7.6 earthquakes occurred in 1987 and 1988 (Lahr et al., 1988; Fletcher and Freymueller, 1999), by internal deformation of the YT, or by deformation inboard of the Fairweather fault, such as along the Denali fault or ~800 km inland to the Mackenzie mountains (Figure 1) (Mazzotti and Hyndman, 2002). Nonetheless, the new thermochronometric data for the Fairweather corridor indicate that a significant component of the plate motion vector must be accommodated elsewhere, be it on the Transition fault or some other structure.

5.3 Temporal variation in exhumation

Late Cenozoic exhumation rates derived from AHe ages in the Fairweather corridor are at least an order of magnitude slower than erosion rates based on short-term (< 100 yr) sedimentation rates recorded in glacial fjords (Figure 24a) (e.g. Hallet et al., 1996). However, modern fjordic sedimentation rates are affected by glacial surges and

retreats, as well as by release of sediment from storage (Koppes and Hallet, 2002; Meigs et al., 2006), and thus, do not provide a good proxy for regional, long-term denudation rate. Holocene erosion rates derived from offshore deposits provide a better estimate of regional denudation. Holocene erosion rates averaged for the region between Cross Sound and Icy Bay based on sediment on the continental shelf are 5.1 mm/yr (± 50%) (Sheaf et al., 2003), or ~5X faster than average AHe-based exhumation rates. As proposed in the Chugach-St. Elias (Spotila et al., 2004), this comparison suggests shorter-term erosion rates are transient and do not reflect denudation over the last few Ma.

Exhumation rates through time are further constrained by K/Ar biotite and hornblende ages. K/Ar ages in the Chugach terrane are significantly older than AHe and AFT ages (Table 1), and are similar to zircon U/Pb crystallization ages where available (~30-50 Ma) (e.g. Hudson et al., 1977; Campbell and Dodds, 1988). This indicates that samples crystallized, and shortly thereafter cooled rapidly to ~350°C. Subsequent exhumation-driven cooling proceeded at slower rates and shorter durations, such that dated samples have not been exhumed from deeper than 12 km (assuming dT/dz = 30°C/km). If exhumation rates have been steady, non-reset K/Ar biotite ages imply that the onset of exhumation recorded by AHe and AFT occurred sometime after ~12 Ma. The implied intervening exhumation rate (i.e. between 12 and 35 Ma) was < 0.35 mm/yr. K/Ar biotite ages in the Wrangellia terrane are even older (Campbell and Dodds, 1988) implying that the mid-Cenozoic Chugach terrane collision resulted in less than 12 km of exhumation in the North American backstop, and that total late Cenozoic exhumation based on young AHe ages has been less than in the Chugach terrane, which is closer to the plate margin (Figure 24b).

This speculative exhumation history provides clues about landscape evolution and the drivers of exhumation in the Fairweather corridor. The proposed regional increase in exhumation rates after 12 Ma is likely when the rugged topography in the Fairweather corridor began to develop. However, at this time the YT abutted the Fairweather corridor and PA-NA motion was parallel to the plate margin (Engebretson et al., 1985). This implies little to drive convergence and denudation during this time. At ~5 Ma, PA-NA motion rotated clockwise (Engebretson et al., 1985), resulting in an obliquity of ~20° between PA motion and the Fairweather corridor . Additionally, regional glaciation

began at approximately the same time (Eyles et al., 1991; Lagoe et al., 1994). It is likely that these changes drove rapid exhumation and relief creation. However, resolving the relative importance of changes in climate and plate motion in driving exhumation is complicated both by their nearly contemporaneous occurrence and by the unknown coupling of the PA and YT through time.

Evidence for an increase in regional exhumation rate since 10 Ma occurs in numerous localities along the 1500-km-long coastal margin of North America, as far south as Washington (Figure 25) (Reiners et al., 2002; Parrish, 1983; Farley et al., 2001; Shuster et al., 2005; Hickes, 2001). The contemporaneous increase in exhumation rate over such a large area has been used to infer climatic control on exhumation (Reiners et al., 2002). Additionally, vertical transects and $^{4}He/^{3}He$ thermochronometry in the Coast mountains of British Columbia and vertical transects in southeast Alaska, resolve an increase in exhumation rate at ~2 Ma (Farley et al., 2001; Shuster et al., 2005; Hickes, 2001). This timing corresponds with increased climate instability following the onset of Northern Hemisphere glaciation (Shuster et al., 2005), and suggests that much of the relief in these areas developed due to glacial erosion. It is plausible that the Fairweather corridor was affected by similar changes in climate, and thus the current topography and exhumation rates may similarly be attributed, in part, to climatic change. However, in contrast to the aforementioned areas, AHe ages in the Fairweather corridor are young at high elevations (e.g. 0.89 Ma, 1610 m) and AFT ages are < 5 Ma, indicating that total exhumation since 5 Ma is significantly greater in the Fairweather corridor (Figure 25). Recent exhumation of > 4km of rock precludes glacial modification of an existing landscape as the sole driver of rapid recent exhumation. Given that tectonic convergence across the plate margin could conceivably generate much more shortening than is observed, it seems reasonable to favor plate tectonics as the primary driver of the observed denudation in the Fairweather corridor. Vertical transects and ages from intermediate T_c systems (e.g. zircon (U-Th)/He) are needed to further constrain the history of exhumation in the region and will allow for a more accurate analysis of the role of climate and tectonics in the denudation of the Fairweather corridor.

5.4 Implications for Transpression

Widespread rapid exhumation in the Fairweather corridor, as revealed by AHe dating, has important implications for transpression in glaciated settings. Distributed exhumation is expected in models of partitioned transpressive deformation (Mount and Suppe, 1987; Tikoff and Teyssier et al., 1994). However, based on the small AHe derived degree of YT-NA obliquity (~5°), the rapidly exhuming zone is more widespread than expected. This may indicate that the Fairweather corridor does not fit existing models of transpression, although assumptions used to derive the 5° obliquity could instead be inaccurate. Rapid exhumation near (< 5 km) the master strike-slip fault (i.e. the Fairweather fault) implies convergent deformation in the near-field. This convergence is not expected in a weak fault, stress-partitioned model, where vertical deformation is restricted to the far-field, and may be more compatible with a strain-partitioned model of transpression (Fossen and Tikoff, 1998; Spotila et al., 2001). However, AHe data are sparse and the inferred exhumation may be partially attributed to glacial erosion rather than to tectonic convergence. Furthermore, the YT-NA obliquity is poorly constrained and the orientation of both the regional stress-field and active structures are unknown. Thus, assessing the validity of transpressive models in the Fairweather corridor is premature given existing data.

Although some of the boundary conditions related to transpression are not yet known for this margin, an interesting comparison can still be made with another similar transpressive zone—the Alpine fault. If we assume perfect PA-YT coupling (i.e. no slip on the Transition fault), the tectonic and climatic inputs in the Fairweather corridor are similar to those in the Southern Alps. Resolved obliquities along the Fairweather and Alpine faults are ~19° and ~18° (Little et al., 2005), respectively, and precipitation rates are 3-10 m/yr in the Fairweather corridor and 2-15 m/yr in New Zealand. Additionally, the heavy precipitation and high latitude location of each results in glacial coverage, although more extensive in Alaska. However, despite the similarities, the resulting topography, structural style, and exhumation patterns are strikingly different between the two areas. Slip partitioning in New Zealand is minor and much of the motion (~70%) is accommodated by oblique-slip along the Alpine fault (Little et al., 2005). In contrast, almost all strike-slip motion (~90-100%) is partitioned onto the Fairweather fault in

Alaska (Fletcher and Freymueller, 2003). Exhumation rates in New Zealand show a distinct increase towards the Alpine fault, whereas rates are similar over a broad zone in Alaska. Furthermore, resolved exhumation rates in New Zealand are more rapid (max. rates of 3 mm/yr in Alaska vs. 9 mm/yr in New Zealand) and deeper crustal levels have been exhumed (e.g. Batt et al., 2000; Little et al., 2005). Numerical modeling indicates that concentrated orographic erosion in a temperature dependent rheology thermally weakens the crust and causes the structural style in oblique settings to evolve from a partitioned system to accommodation along a single oblique-slip structure (Koons et al., 2003). If this model is correct it implies that total exhumation in the Fairweather corridor has not been sufficient to weaken the crust and concentrate motion on a single structure. Possible causes of low total exhumation include obliquity significantly less than 19° due to slip on the transition fault (as implied by shortening derived from AHe data), less concentrated orographic erosion than in New Zealand, and short total time of oblique convergence.

Figure Captions:

Figure 22: Exhumation rates derived from AHe ages and assumed closure depths of 1.9-2.5 km plotted on a 3-D view of the Fairweather corridor. Bar heights correspond to exhumation rate. Image was created using ArcScene and the elevation data are from the USGS and available online.

Figure 23: a) Geometry of plate motion with respect to the Fairweather corridor. Area of exhumation is defined by AHe derived exhumation rates, and YT thickness is taken from the cross section of Plafker et al. (1994) (PA-NA from DeMets and Dixon, 1999). b) Schematic showing mass balance in the Fairweather corridor between accretionary influx and exhumational efflux; 4.3 mm/yr of convergence is required for the influx to match efflux (flux steady-state). c) The convergence rate coupled with either geologic (Plafker et al., 1978) or geodetic (Fletcher and Freymueller, 2003) constraints on the Fairweather defines the resultant vector of YT-NA motion and the unaccommodated plate motion.

Figure 24: a) Inferred erosion rate versus the time scale of the observation. Short-term erosion rates (Hallet et al., 1996; Sheaf et al., 2003) are anomalously high compared to million-year averages from thermochronologic data. b) Late Cenozoic erosion rates are greater than longer-term erosion rates derived from K/Ar ages (Hudson et al., 1977; Dodds and Campbell, 1988). The onset of rapid exhumation is constrained at < 12 Ma by ages and likely occurred at 5 Ma when changes in both climate and tectonics occurred. K/Ar ages in the North American backstop indicate extremely slow protracted cooling.

Figure 25: Thermochronologic ages of sea-level samples from Washington to southeast Alaska. Shaded area encompasses AHe average ages from Juneau southwards. Glacier Bay samples are from sea-level and can be directly compared to the other data, samples north of the Alsek River range in elevation. AHe average ages from this study are significantly younger than elsewhere (dashed line). Additionally, AFT age (O'Sullivan et al., 1997) shows a sharp decrease from Juneau to the Fairweather corridor (dotted line) indicating greater total exhumation. Data from Reiners et al. (2002), and references therein.

Figure 22

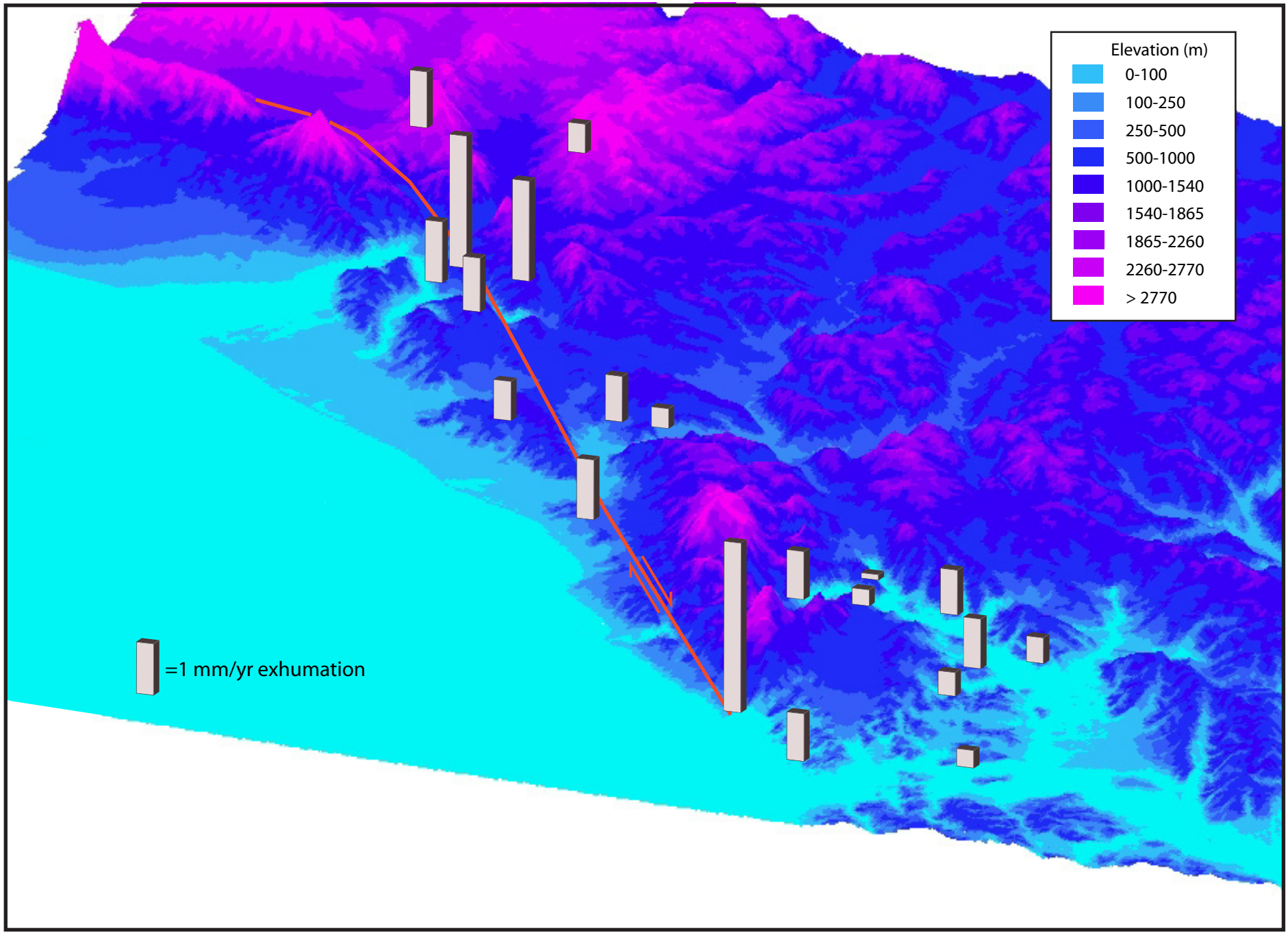
Elevation (m)
0-100
100-250
250-500
500-1000
1000-1540
1540-1865
1865-2260
2260-2770
> 2770
=1 mm/yr exhumation

Figure 23

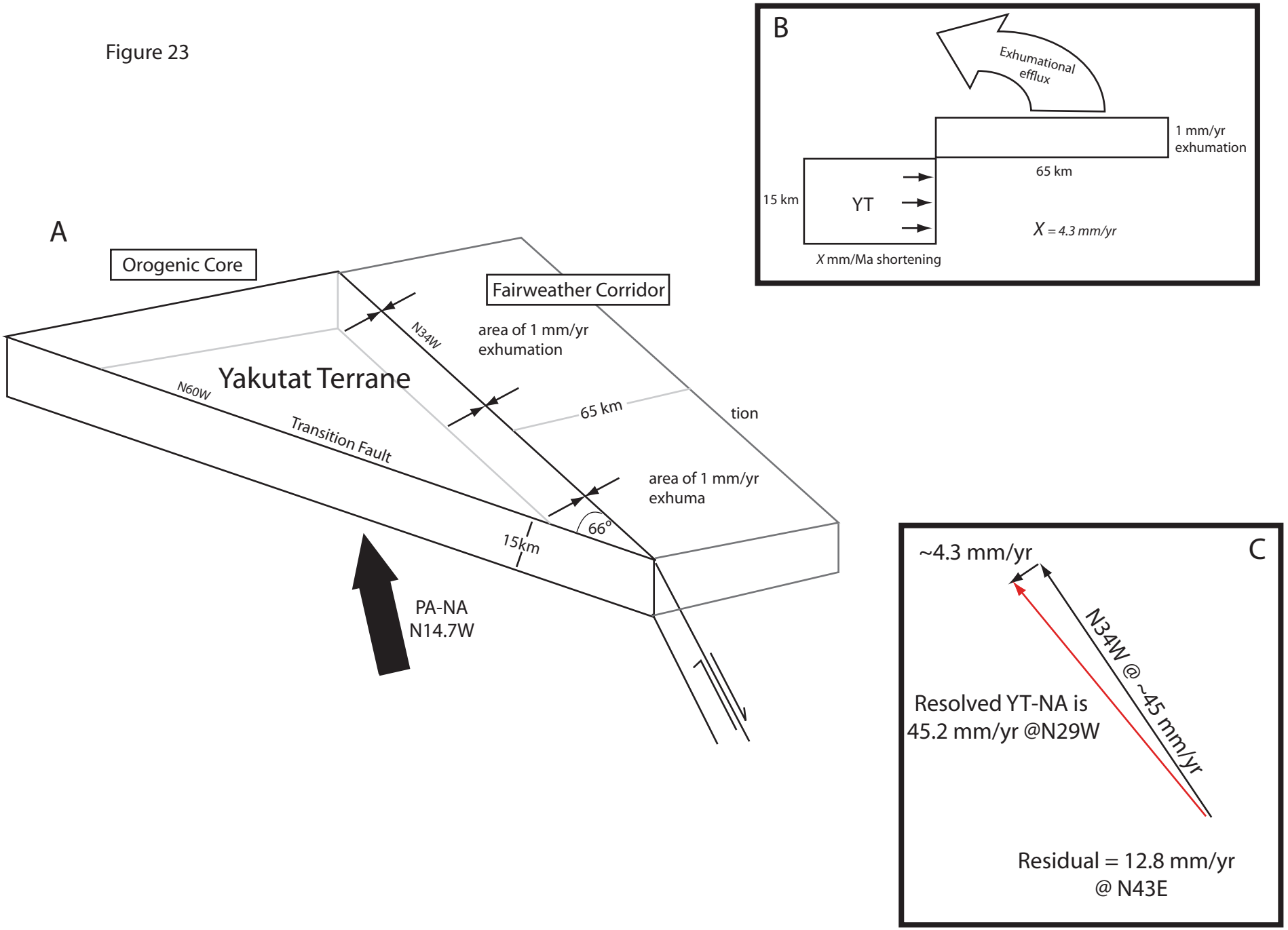
A
Orogenic Core
Fairweather Corridor
N34W
area of 1 mm/yr
exhumation
Yakutat Terrane
N60W
Transition Fault
65 km
tion
area of 1 mm/yr
exhuma
66°
15km
PA-NA
N14.7W
B
Exhumational
efflux
1 mm/yr
exhumation
65 km
15 km
YT
X = 4.3 mm/yr
X mm/Ma shortening
C
~4.3 mm/yr
N34W @ ~45 mm/yr
Resolved YT-NA is
45.2 mm/yr @N29W
Residual = 12.8 mm/yr
@ N43E

Figure 24

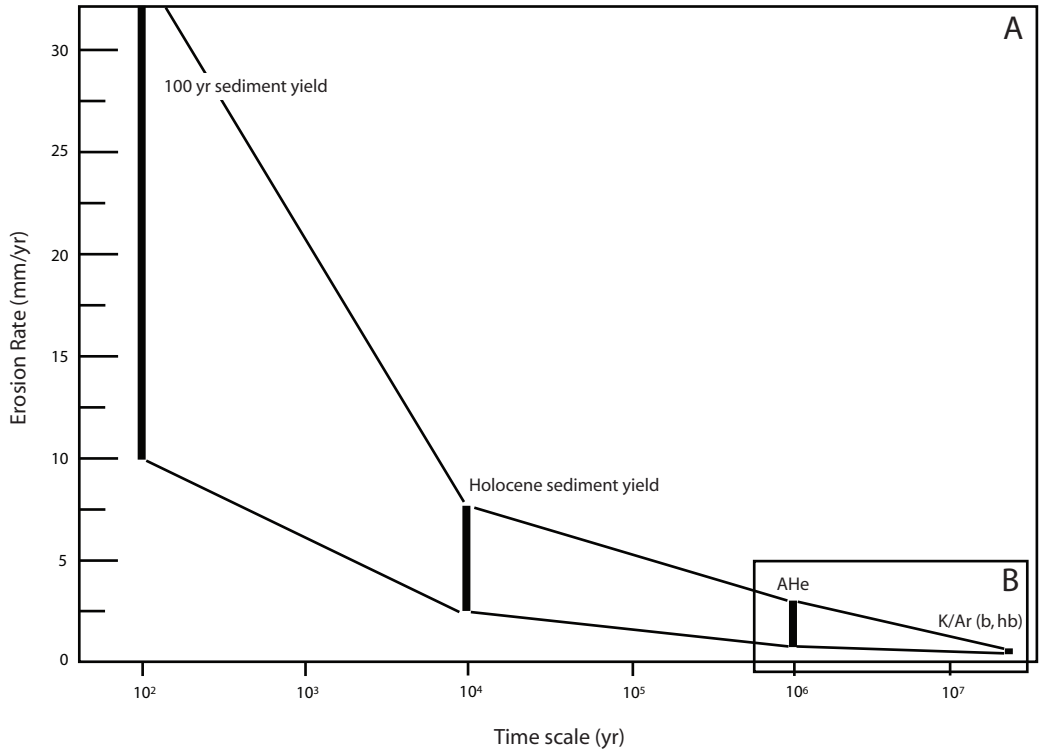
A
100 yr sediment yield
Holocene sediment yield
AHe
B
K/Ar (b, hb)
Erosion Rate (mm/yr)
30
25
20
15
10
5
0
10^2
10^3
10^4
10^5
10^6
10^7
Time scale (yr)

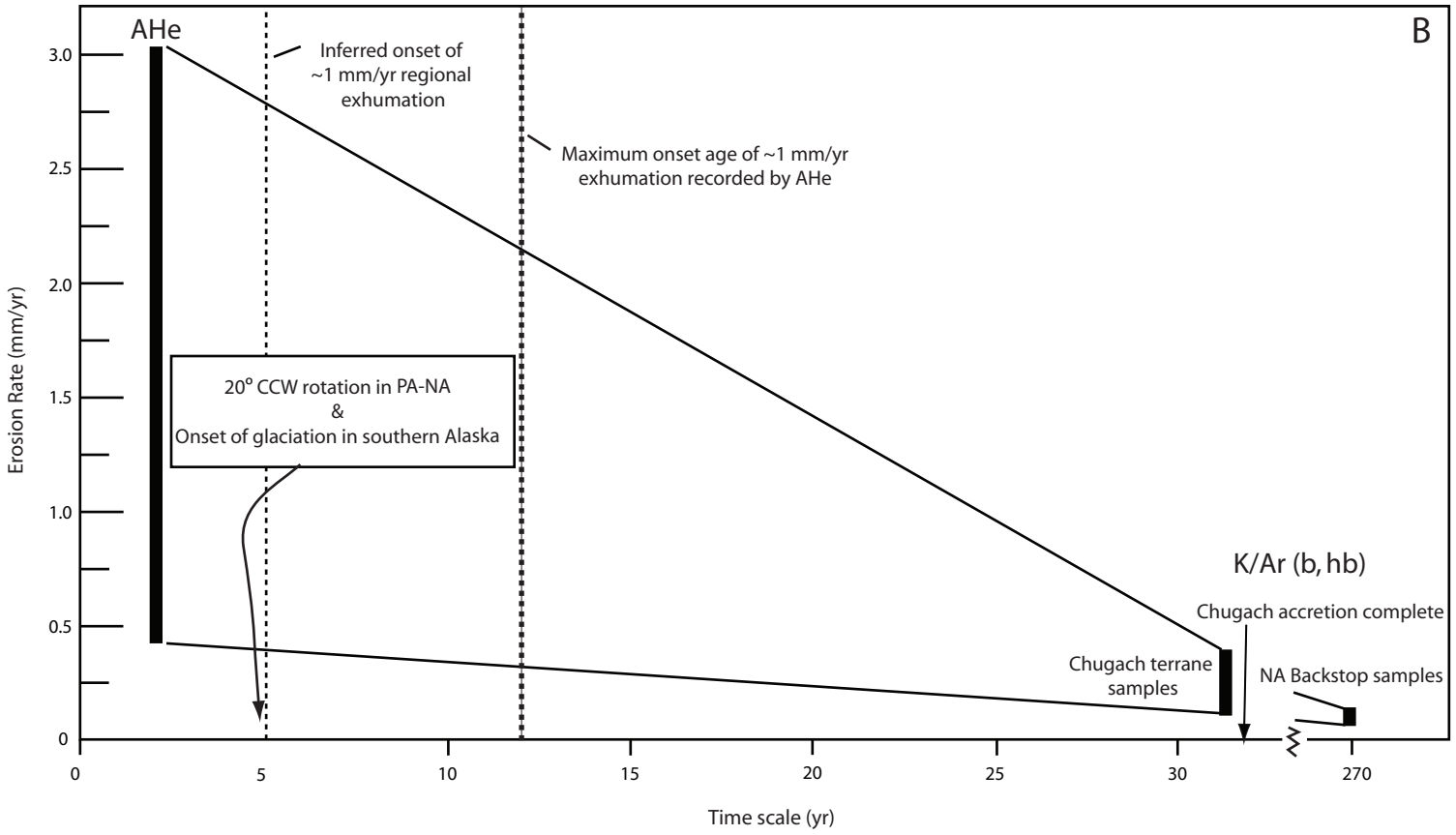
AHe
B
Inferred onset of
~1 mm/yr regional
exhumation
Maximum onset age of ~1 mm/yr
exhumation recorded by AHe
20° CCW rotation in PA-NA
&
Onset of glaciation in southern Alaska
K/Ar (b, hb)
Chugach accretion complete
Chugach terrane
samples
NA Backstop samples
Erosion Rate (mm/yr)
3.0
2.5
2.0
1.5
1.0
0.5
0
0
5
10
15
20
25
30
270
Time scale (yr)

Figure 25

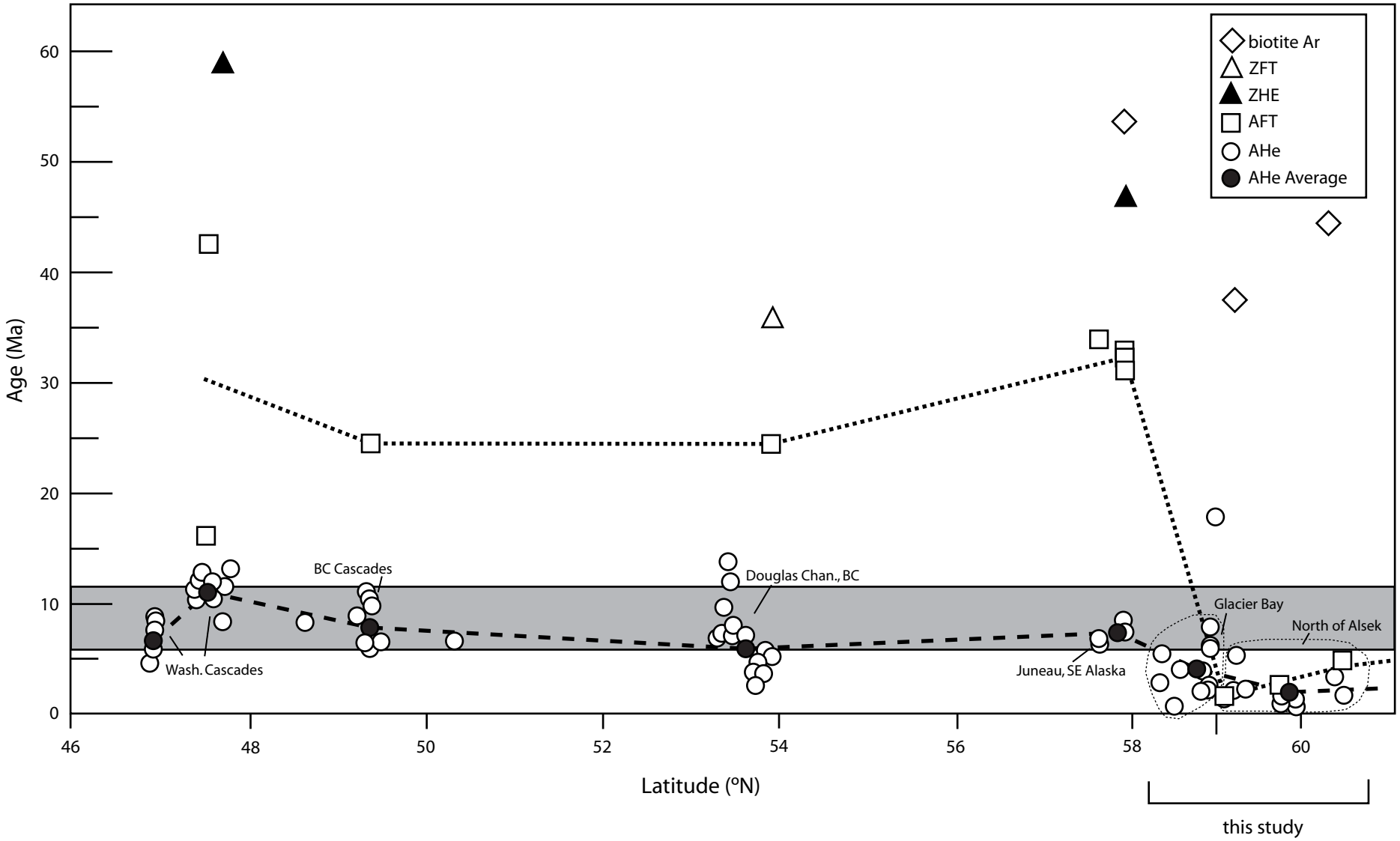
biotite Ar
ZFT
ZHE
AFT
AHe
AHe Average
Age (Ma)
0
10
20
30
40
50
60
46
48
50
52
54
56
58
60
Latitude (ºN)
BC Cascades
Douglas Chan., BC
Glacier Bay
North of Alsek
Wash. Cascades
Juneau, SE Alaska
this study

6. Conclusions

Young AHe cooling ages occur in a broad zone along the trace of the Fairweather fault. Ages correspond to a regional exhumation rate of ~1 mm/yr and peak rates of ~3 mm/yr, indicating that convergence has been accommodated in the Fairweather corridor over the past few Ma. A rough estimate of the convergence required to produce observed exhumation is only a small fraction of the 16.8 mm/yr Fairweather-normal component of PA-NA motion, and requires convergence elsewhere. Additionally, similar to modern GPS, this estimate indicates that the YT and PA are decoupled, with YT-NA motion rotated ~14° from PA-NA the vector. Convergence and decoupling likely occur at the Transition fault, however, uncertainties in the convergence estimate, and the unknown nature of the Transition fault make assignment of motion equivocal.

Thermochronologic data constrain the onset of ~1 mm/yr exhumation to post-12 Ma, and constrain prior rates to < 0.35 mm/yr in the Chugach terrane and much slower inboard. Although age data do not further restrict the onset of rapid exhumation the tectonic and climatic changes at ~5 Ma likely affected rates. AFT and AHe ages preclude glacial modification of the landscape as the sole driver of exhumation, as is proposed in the Coast Ranges. Additionally, AHe derived exhumation rates are significantly slower than short-term erosion rates, and highlight the transient nature of erosion during deglaciation. More data are needed to further constrain temporal changes in exhumation and the long-term, relative effects of climate and tectonics in the Fairweather corridor.

Exhumation rates indicate that the margin accommodates pure shear deformation, and that motion must be partitioned between the observed strike-slip motion on the Fairweather fault and shortening on other structures. However, no coherent regional pattern of exhumation is evident, and exhumation is surprisingly widespread based on the AHe derived obliquity. Rapid exhumation near the fault may be more compatible with a strain-partitioned model of transpression, however, sparse sampling and the many unknowns of the Fairwather corridor make this assessment tenuous.

References Cited

Batt, G.E., Braun J., Kohn B.P., and McDougall, I., 2000, Thermochronological analysis of the dynamics of the Southern Alps, New Zealand: Geological Society of America Bulletin, v. 112, p. 250-266.

Beaumont, C., Fullsack, P., and Hamilton J., 1992, Erosional control of active compressional orogens, in McClay, K.R. ed., Thrust tectonics: New York, Chapman and Hall, p. 1-18.

Bird, P., 1996, Computer simulations of Alaskan neotectonics: Tectonics, v. 15, p. 225-236.

Dodds, C.J, and Campbell, R.B., 1988, Potassium-argon ages of mainly intrusive rocks in the Saint Elias Mountains, Yukon and British Columbia: Geological Survey of Canada Paper 87, p. 1–43.

Carlson, P.R., Bruns, T.R., and Plafker, G., 1988, Late Cenozoic offsets on the offshore connection between the Fairweather and Queen Charlotte faults off southeast Alaska: Marine Geology, v. 85, p. 89-97.

DeMets, C., Gordon, R.C., Argus, D.F., and Stein, S., 1994, Effect of recent revisions to the geomagnetic reversal time scale on estimates of current plate motions: Geophysical Research Letters, v. 21, p. 2191–2194.

DeMets, C., and Dixon, T., 1999, New kinematic models for Pacific-North America motion from 3 Ma to present, I. Evidence for steady motion and biases in the NUVEL-1A model: Geophyscial Research Letters, v. 26, p. 1921-1924.

Dodson, M.H., 1973, Closure temperatures in cooling geological and petrological systems: Contributions in Mineralogy and Petrology, v. 40, p. 259-274.

Doser, D.I., and Lomas, R., 2000, The transition from strike-slip to oblique subduction in southeastern Alaska from seismological studies: Tectonophysics, v. 316, p. 45–65.

Doser, D.I., Pelton, J.R., and Veilleux, A.M., 1997, Earthquakes in the Pamplona zone, Yakutat Block, southcentral Alaska: Journal of Geophysical Research, v. 102, p. 24499–24511.

Eberhart-Phillips, D., and 28 others, 2003, The 2002 Denali fault earthquake, Alaska: a large magnitude slip-partitioned event: Science, v. 300 , p. 1113 –1118.

Ehlers, T.A., 2005, Crustal thermal processes and the interpretation of thermochronometer data, *in* Ehlers, T., and Reiners, P.W., eds., Low temperature thermochronometry: Techniques, interpretations, and applications: Reviews in

Mineralogy and Geochemistry, Mineralogical Society of America, v. 58, p. 315-350.

Ehlers, T.A., and Farley, K.A., 2003, Apatite (U-Th)/He thermochronometry: methods and applications to problems in tectonic and surface processes: Earth and Planetary Science Letters, v. 206, p. 1-14.

Eyles, C.H., Eyles, N., and Lagoe, M.N., 1991, The Yakataga Formation: A late Miocene to Pleistocene record of temperate glacial marine sedimentation: *in* Anderson, J.B., and Ashley, G.M., eds., The Gulf of Alaska: Geological Society of America Special Paper 261, p. 159–187.

Farley, K.A., 2000, Helium diffusion from apatite: general behavior as illustrated by Durango fluorapatite: Journal of Geophysical Research, v. 105, p. 2903-2914.

Farley, K.A., 2002, (U-Th)/He dating: techniques, calibrations and applications: Review in Mineralogy and Geochemistry, v. 47, p. 819-844.

Farley, K.A., Rusmore, M.E., and Bogue, S.W., 2001, Post–10 Ma uplift and exhumation of the northern Coast Mountains, British Columbia: Geology, v. 29, p. 99–102.

Farley, K.A., Wolf, R.A., and Silver, L.T., 1996, The effects of long alpha-stopping distances on (U-Th)/He ages: Geochimica et Cosmochimica Acta, v. 60, p. 4223-4229.

Fletcher, H.J., and Freymueller, J.T., 1999, New GPS constraints on the motion of the Yakutat Block: Geophysical Research Letters, v. 26, p. 3029–3032.

Fletcher, H.J., and Freymueller, J.T., 2003, New constraints on the motion of the Fairweather fault, Alaska, from GPS observations: Geophysical Research Letters, v. 30, p. 1139–1142.

Flett, T.O., 1992, Temperature gradients, *in* Turner, R.F., ed., Geologic report for the Gulf of Alaska planning area: Minerals Management Service OCS Report MMS 92-0065, 302 p.

Fossen, H., and Tikoff, B, 1998, Extended models of transpression and transtension, and application to tectonic settings. In: Holdsworth, R.E., Strachan, R.A. and Dewey, J.F. (eds.), Continental transpressional and transtensional tectonics. Geol. Soc. Lond. Spec. Publ. v. 135, p. 15-33.

Hallet, B., Hunter, L., and Bogen, J., 1996, Rates of erosion and sediment evacuation by glaciers: A review of field data and their implications: Global and Planetary Change, v. 12, p. 213–235.

Hickes, H.J., 2001, Apatite and zircon (U-Th)/He thermochronology of the northern Coast Mountains, southeast Alaska [M.S. thesis]: Pullman, Washington State University, 47 p.

House, M.A., Gurnis, M., Kamp, P.J., and Sutherland, R., 2002, Uplift in Fiordland region, New Zealand: Implications for incipient subduction: Science, v. 297, p. 2038-2041.

Hudson, T., Plafker, G. and Rubin, M., 1976. Uplift rates of marine terrace sequences in the Gulf of Alaska. In: Cobb, E.H., Editor, 1976. The United States Geological Survey in Alaska: Accomplishments during 1975, United States Geological Survey, Denver, p. 11–13.

Hudson T., Plafker, M.A., and Lanphere, M.A., 1977, Intrusive rocks of the Yakutat-Saint Elias area, south-central Alaska: United States Geological Survey Journal of Research, v. 5, p. 15-172.

Jaeger, J.M., Hallet, B., Pavlis, T., Sauber, J., Lawson, D., Milliman, J., Anderson, S., and Anderson, R., 2001, Orogenic and glacial research in pristine southern Alaska [abs]: Eos (Transactions, American Geophysical Union), v. 82, p. 213–216.

Johnsson, M.J., Pawlewicz, M.J., Harris, A.G., and Valin, Z.C., 1992, Vitrinite reflectance and conodont color alteration index data from Alaska: data to accompany the thermal maturity map of Alaska, United State Geological Survey Open-File Report 92-409.

Hickes, H.J., 2001, Apatite and zircon (U-Th)/He thermochronology of the northern Coast Mountains, southeast Alaska [M.S. thesis]: Pullman, Washington State University, 47 p.

Johnston, S.A., 2005, Geologic structure and exhumation accompanying Yakutat Terrane collision, Southern Alaska [M.S. thesis]: Corvallis, Oregon State University, 49 p.

Koons, P.O., Norris, R.J., Craw, D., and Cooper, A.F., 2003, Influence of exhumation on the structural evolution of transpressional plate boundaries; An example from the Southern Alps, New Zealand: Geology, v. 31, p. 3-6.

Koppes, M.N., and Hallet., B., 2002, Influence of rapid glacial retreat on the rate of erosion by tidewater glaciers: Geology v. 30, p. 47-50.

Lagoe, M.B., Eyles, C.H., Eyles, N., and Hale, C., 1993, Timing of late Cenozoic tidewater glaciation in the far North Pacific: Geological Society of America Bulletin, v. 105, p. 1542–1560.

Lahr, J.C., and Plafker, G., 1980, Holocene Pacific–North American plate interaction in southern Alaska: Implications for the Yakataga seismic gap: Geology, v. 8, p. 483–486.

Lahr, J.C., Page, R.A., Stephens, C.D., and Christensen, D.H., 1988, Unusual earthquakes in the Gulf of Alaska and fragmentation of the Pacific Plate: Geophysical Research Letters, v. 15, p. 1483–1486.

Larsen, C.F., Echelmeyer K.A., Freymueller J.T., and Motyka R.J., 2003, Tide gauge records of uplift along the northern Pacific-North American plate boundary, 1937 to 2001: Journal of Geophysical Research, v. 108, p. 2216.

Larsen, C.F., Motyka, R.J., Freymueller, J.T., Echelmeyer, K.A., and Ivins, E.R., 2004, Rapid uplift of southern Alaska caused by recent ice loss: Geophyiscal Journal International, v. 158, p. 1118-1133.

Larsen, C.F., Motyka, R.J., Freymueller, J.T., Echelmeyer, K.A., and Ivins, E.R., 2005, Rapid viscoelastic uplift in southeast Alaska caused by post-Little Ice Age glacial retreat: Earth and Planetary Science Letters, v. 237, p. 548-560.

Lisowski, M., Savage, J.C., and Burford, R.O., 1987, Strain accumulation across the Fairweather and Totschunda faults, Alaska: Journal of Geophysical Research, v. 92, p. 11552–11560.

Little, T.A., Cox, S., Vry, J.K., and Batt, G., 2005, Variations in exhumation level and uplift rate along the oblique-slip Alpine fault, central Southern Alps, New Zealand: Geological Society of America Bulletin, v. 117, 707–723.

Lundgren, P., Saucier, F., Palmer, R., and Langon, M., 1995, Alaska crustal deformation: Finite element modeling constrained by geologic and very long baseline interferometry data: Journal of Geophysical Research, v. 100, 22033–22045.

Mancktelow, N.S., and Grasemann, B., 1997, Time-dependant effects of heat advection on topography on cooling histories during erosion: Tectonophysics, v. 270, p. 167-195.

Mazzotti, S., and Hyndman, R.D., 2002, Yakutat collision and strain transfer across the across the northern Canadian Cordillera: Geology, v. 30, p. 495-498.

McDougall, I., and Harrison, T.M., 1999, Geochronology and thermochronology by the $^{40}Ar/^{39}Ar$ method. Oxford University Press, New York.

Meigs, A., Krugh, W.C., Davis, K., and Bank, G., 2006 (in press), Ultra-rapid landscape response and sediment yield following glacier retreat, Icy Bay southern Alaska: Geomorphology, 15 p.

Mount, V.S., and Suppe, J., 1987, State of stress near the San Andreas fault: Implications for wrench tectonics: Geology, v. 15, p. 1143-1146.

Norris, R.J., and Cooper, A.F., 2001, Late Quaternary slip rates and slip partitioning on the Alpine fault, New Zealand: Journal of Structural Geology, v. 23, p. 507–520.

O'Sullivan, P.B., and Currie, L.D., 1996, Thermotectonic history of Mt. Logan, Yukon Territory, Canada: Implications of multiple episodes of middle to late Cenozoic denudation: Earth and Planetary Science Letters, v. 144, 251–261.

O'Sullivan, P.B., Plafker, G., and Murphy, J.M., 1997, Apatite fission-track thermotectonic history of crystalline rocks in the northern St. Elias Mountains, Alaska, in Dumoulin, J.A., and Gray, J.E., eds., Geological studies *in* Alaska by the United States Geological Survey, 1995: United States Geological Survey Professional Paper 1574, p. 283-294.

Page, R.A., 1969, Late Cenozoic movement on the Fairweather fault in southeast Alaska: Geological Society of America Bulletin, v. 80, p. 1873-1878.

Parrish, R.R., 1983, Cenozoic thermal evolution and tectonics of the Coast Mountains of British Columbia: 1. Fission track dating, apparent uplift rates, and patterns of uplift: Tectonics, v. 2, p. 601–631.

Pavlis, G.L., Picornell, C., Serpa, L., Bruhn., R.L., and Plafker, G., 2004, Tectonic processes during oblique collision: Insights from the St. Elias orogen, northern North American Cordillera: Tectonics, v. 23, TC3001, p. 1-14.

Plafker, G., and Thatcher, W., 1982, Geological and geophysical evaluation of the mechanisms of the great 1899–1900 Yakutat Bay, Alaska earthquakes [abs]: Snowbird, Utah, American Geophysical Union Conference on Fault Behavior and Earthquake Generating Processes, Oct. 11–15.

Plafker, G., Hudson, T., Bruns, T.R., and Rubin, M., 1978, Late Quaternary offsets along the Fairweather Fault and crustal plate interactions in southern Alaska: Canadian Journal of Earth Sciences, v. 15, p. 805–816.

Plafker, G., Moore, J.C., and Winkler, G.R., 1994, Geology of the southern Alaska margin, *in* Plafker, G., and Berg, H.C., eds., The geology of Alaska: Boulder, Colorado, Geological Society of America, Geology of North America, G-1, 389–449.

Reiners, P.W., Ehlers, T.A., Garver, J.I., Mitchell, S.G., Montgomery, D.R., Vance, J.A., and Nicolescu, S., 2002, Late Miocene exhumation and uplift of the Washington Cascades: Geology, v. 30, p. 767–770.

Reiners, P.W., Zhou, Z., Ehlers, T.A., Xu, C., Brandon, M.T., Donelick, R.A., and Nicolescu, S., 2003, Post-orogenic evolution of the Dabie Shan, eastern China, from (U-Th)/He and fission-track dating: American Journal of Science, v. 303, p. 489-518.

Reiners, P.W., Ehlers, T.A., and Zeitler, P.K., 2005, Past, Present, and Future of Thermochronology, in Reiners, P.W. and Ehlers, T.A. (Eds.), Thermochronology, Reviews in Mineralogy and Geochemistry, v. 58, p. 1-18.

Roeske, S.M., Pavlis, T.L., Snee, L.W., and Sisson, V.B., 1992, $^{40}Ar/^{39}Ar$ isotopic ages from the combined Wrangellia-Alexander terrane along the Border Ranges fault system in the eastern Chugach Mountains and Glacier Bay, Alaska, *in* Bradley, D.C., and Ford, A.B., eds., Geologic studies in Alaska by the U.S. Geological Survey, 1990: U.S. Geological Survey Bulletin 1999, p. 180–195.

Sauber, J., McClusky, S., and King, R., 1997, Relation of ongoing deformation rates to the subduction zone process in southern Alaska: Geophysical Research Letters, v. 24, p. 2853–2856.

Schneider, D.A., Edwards, M.A., Kidd, W.S.F., Khan, M.A., Seeber, L., and Zeitler, P.K., 1999, Tectonics of Nanga Parbat, western Himalaya: Synkinematic plutonism within the doubly vergent shear zones of a crustal-scale pop-up structure: Geology, v. 27, p. 999–1002.

Searle, M.P., Parrish, R.E., Hodges, K.V., Hurford, A., Ayres, M.W., Whitehouse, M.J., 1997, Shisha Pangma leucogranite, South Tibetan Himalaya: Field relations, geochemistry, age, origin and emplacement: Journal of Geology, v. 105, p. 295-317.

Sheaf, M.A., Serpa, L., and Pavlis, T.L., 2003, Exhumation rates in the St. Elias Mountains, Alaska: Tectonophysics, v.367, p. 1–11.

Shuster, D.L., Ehlers, T.A., Rusmoren, M.E., and Farley, K.A., 2005, Rapid glacial erosion at 1.8 Ma revealed by $^{4}He/^{3}He$ thermochronometry: Science, v. 310, p. 1668-1670.

Smart, K.J., Pavlis, T.L., Sisson, V.B., Roeske, S.M., and Snee, L.W., 1996, The Border Ranges fault system in Glacier Bay National Park, Alaska: Evidence for major early Cenozoic dextral strike-slip motion: Canadian Journal of Earth Sciences, v. 33, p. 1268–1282.

Spotila, J.A., Farley, K., Yule, D., and Reiners, P., 2001, Near-field transpressive deformation along the San Andreas fault zone in southern California, based on exhumation constrained by (U-Th)/He dating: Journal of Geophysical Research, v. 106, p. 30,909-30922.

Spotila, J.A., Buscher, J.T., Meigs, A.J., and Reiners, P.W., 2004, Long-term glacial erosion of active mountain belts: Example of the Chugach-St. Elias Range, Alaska: Geology, v. 32, p. 501–504.

Spotila, J., Bank, G., Naeser, C., Naeser, N., Reiners, P., and Henika, B., 2004, Origin of the Blue Ridge escarpment along the passive margin of eastern United States: Basin Research, v. 16, p. 41-63.

Spotila, J.A., 2005, Applications of low-temperature thermochronometry to quantification of recent exhumation in mountain belts, *in* Ehlers, T., and Reiners, P.W., eds., Low temperature thermochronometry: Techniques, interpretations, and applications: Reviews in Mineralogy and Geochemistry, Mineralogical Society of America, v. 58, p. 449-466.

Stockli, D.F., Farley, K.A. and Dumitru, T.A., 2000, Calibration of the (U-Th)/He thermochronometer on an exhumed normal fault block in the White Mountains, eastern California and western Nevada: Geology, v. 28, p.983-986.

Strutt, R.J., 1908, The accumulation of helium in geologic time. Processions of the Royal Society of London, p. 272-277.

Stuwe K.L., White, L., and Brown, R., 1994, The influence of eroding topography on steady-state isotherms: application to fission-track analysis: Earth and Planetary Science Letters, v. 124, p. 63-74.

Tarr, R.S., and Martin, L., 1912, The earthquakes of Yakutat Bay, Alaska in September 1899: U.S. Geological Survey Professional Paper 69. 135 p.

Teyssier, C., Tikoff, B., and Markely, M., 1995, Oblique plate motion and continental tectonics: Geology, v. 23, p. 447-450.

Tikoff, B., and Teyssier, C., 1994, Strain modeling of displacement-field partitioning in transpressional orogens: Journal of Structural Geology, v. 16, p. 1575-1588.

Tocher, D., and Miller, D., 1959, Field observations on effects of the Alaska earthquake of 10 July 1958: Science, v. 129, p. 395-396.

Vauchez, A., and Nicolas, A., 1991, Mountain building: Strike parallel motion and mantle anisotropy: Tectonophysics, v. 185, p. 183–201.

Willett, S. D., Beaumont, C. and Fullsack, P., 1993, A mechanical model for the tectonics of doubly vergent compressional orogens: Geology, v. 21, p. 371-374.

Willett, S.D., and Brandon, M.T., 2002, On steady state in mountain belts: Geology, 30, 175–178.Wolf et al 1996

Zeitler, P.K., Herczeg, A.L., McDougall, I., and Honda, M., 1987, U-Th-He dating of apatite: a potential thermochronometer: Geochimica Cosmochimica Acta, v. 51, p. 2865-2868.

Vita

Ryan Joseph McAleer was born in Erie, Pennsylvania in 1982. He graduated from Fairview High School in Fairview, Pennsylvania in 2000. He received a Bachelor of Science degree in 2004 in Geology from The Pennsylvania State University, earning High Honors. Ryan then moved on to Virginia Tech where he received his Master of Science degree in Geology in 2006. He anticipates publishing his thesis work in the near future. His life plans are somewhat more nebulous, but he hopes to at some point break 70 and try many new and interesting foods.